ORNL/TM-2023/2846

Facility to Alleviate Salt Technology Risks (FASTR): Commissioning Update

Kevin Robb
Ethan Kappes

February 2023

Approved for public release.
Distribution is unlimited.

OAK RIDGE National Laboratory

ORNL IS MANAGED BY UT-BATTELLE LLC FOR THE US DEPARTMENT OF ENERGY

ORNL/TM-2023/2846

Nuclear Energy and Fuel Cycle Division

FACILITY TO ALLEVIATE SALT TECHNOLOGY RISKS (FASTR): COMMISSIONING UPDATE

Kevin Robb
Ethan Kappes

February 2023

Prepared by
OAK RIDGE NATIONAL LABORATORY
Oak Ridge, TN 37831
managed by
UT-BATTELLE, LLC
for the
US DEPARTMENT OF ENERGY
under contract DE-AC05-00OR22725

CONTENTS

LIST OF FIGURES

LIST OF TABLES

ABBREVIATIONS

BNL	Brookhaven National Laboratory
CSP	concentrated solar power
DOE	US Department of Energy
FASTR	Facility to Alleviate Salt Technology Risks
Gen 3	Generation 3
HX	heat exchanger
I&C	instrumentation and controls
kPa	kiloPascals
kW	kiloWatt
lpm	liters per minute
NA	not available
PLC	programmable logic controller
psig	pounds per square inch gauge
RGA	residual gas analyzer
sch	schedule (pipe)
sCO_2	supercritical carbon dioxide
SS	stainless steel
TC	thermocouple
UA	University of Arizona
UW	University of Wisconsin

ACKNOWLEDGMENTS

The material presented here is based upon work supported by the US Department of Energy (DOE) Office of Energy Efficiency and Renewable Energy under Solar Energy Technologies Office Agreement Number 33875.

ABSTRACT

The Facility to Alleviate Salt Technology Risks (FASTR) is a versatile, high-temperature (>600°C) molten chloride salt test facility designed to enable a variety of testing to advance the Generation 3 concentrating solar power molten salt technology. FASTR includes a salt preparation system and a forced-flow test loop with a suite of instrumentation. The FASTR loop can operate at 725°C with flow rates of 3–7 kg/s, and it includes heated and cooled sections and swappable components to facilitate testing of future vendor-supplied hardware. The salt preparation system supplies large batches of clean salt for use in the FASTR forced-circulation loop. This report summarizes the shakedown and initial operation of the FASTR forced-circulation loop through December 2022.

1. INTRODUCTION

The Facility to Alleviate Salt Technology Risks (FASTR) is a versatile, high-temperature (>600°C) molten chloride salt test facility designed to enable a variety of testing to advance the Generation 3 (Gen 3) concentrated solar power (CSP) molten salt technology. Before a chloride salt–based Gen 3 CSP plant is deployed, several technological challenges must be resolved, and several capabilities must be demonstrated, including salt sourcing, preparation, and monitoring; component design, supply chain, and reliability; and corrosion control [1]. Very few test facilities are available to mature and de-risk the required technology for molten chloride salts. To address this need, the Solar Energy Technologies Office of the US Department of Energy (DOE) Office of Energy Efficiency and Renewable Energy sponsored the development, construction, and initial operation of FASTR.

FASTR includes a salt preparation system and a forced-flow test loop with a suite of instrumentation. The forced-circulation loop can operate at 725°C with flow rates of 3–7 kg/s. FASTR includes heated and cooled sections and swappable components to enable testing of future vendor-supplied hardware. The salt preparation system supplies large batches (e.g., 200 kg) of clean salt for use in the forced-circulation loop. Key facility demonstrations include corrosion monitoring and control, as well as performance demonstrations of major components such as flanges, heat trace, heat exchangers, pumps, and instrumentation.

The 2019 preliminary facility design presented by Robb et al. [2] describes a failure modes and effects analysis that was conducted to inform design choices and to reduce risks during operation. The salt preparation system and its initial operation are described in the 2022 report by Robb et al. [3]. Finally, a revised design report was published summarizing FASTR's as-built design and capabilities [4]. The current report summarizes the commissioning activities for the convection loop, beginning with shakedown operations up to the initial molten salt pumped operation.

A schematic of FASTR is provided in Figure 1, and an image of the as-built system is shown in Figure 2. FASTR's key technical specifications and capabilities are summarized in Table 1. Finally, the instrumentation and controls (I&C) capabilities are summarized separately in Table 2.

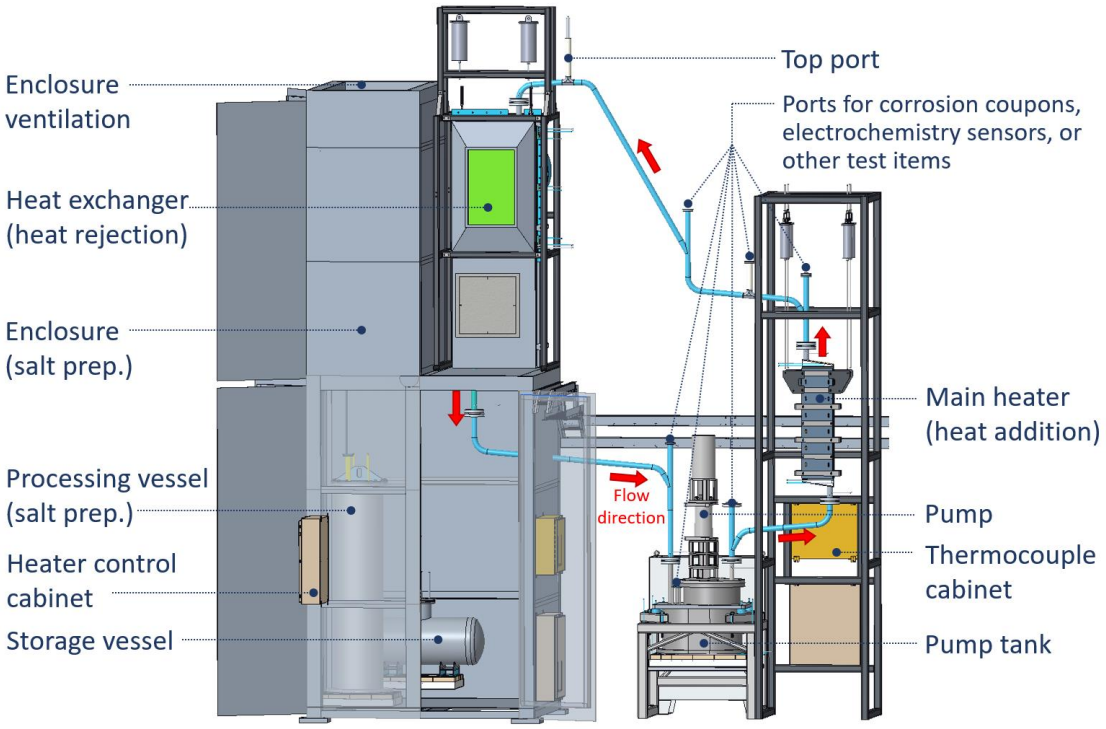

Figure 1. FASTR layout.

Figure 2. FASTR flow loop.

Table 1. FASTR requirements and capabilities

Capability	Detail		Value	Units	Comments
System design temperature	Hot side		725	°C	—
Primary alloys of construction	—		C-276 600	—	—
Primary piping diameter	—		2	in.	Schedule 40, seamless
System design pressure	Salt processing		206	kPa	30 psig
	Flow loop		145–310	kPa	21–45 psig
Salt flow rate	Mass flow rate		3–7	kg/s	3–6 kg/s is primary goal
	Volume flow rate		114–228	lpm	30–70 GPM
Salt volume/mass	Purification system		≥200	kg	If loaded as powder/granules
	Salt loop		154[a]	L	254 kg (~40 gallon)
Main heater	Power	Capacity	400	kW_{th}	To the salt
		Current heaters	103	kW_{th}	144 kW_e with assumed 72% efficiency of energy delivered to test section
	Max. heat flux	Design	1,000	kW/m^2	To the salt
		Current heaters	580	kW/m^2	Estimated
	Axial zones		6	qty	—
	Reynolds number (salt)		15,000–50,000	—	In channels, based on estimated salt properties
Trace heating	Controlled zones		48	qty	—
	Total power		71	kW	—
Test ports	Locations		6	qty	3× hot zone, 3× cold zone (e.g., corrosion samples, sensors)

[a]Additional salt was added to the loop as summarized in Section 3.1.

Table 2. FASTR instrumentation suite

Instrumentation suite	Detail	Qty	Units
Pressure	Gas space	6	Places
Gas mass flow controller	Gas space	12	Places
Salt flow rate	Ultrasonic	1[a]	Places
Salt level	Thermocouple probe	4[b]	Places
Hazardous gas detectors	HCl & Cl_2	3	Places
	H_2	2	Places
pH	System off-gas	1	Places
Residual gas analyzer (RGA)	System off-gas	1	Places
Temperature: thermocouples	Main heater	48	qty
	Trace heating	89	qty
	Flowmeter	2	qty
	Heat exchanger	21	qty
	Level probes	40	qty
	Total	200	qty
Salt redox potential and specie concentrations	Multielectrode array voltammetry sensor with dynamic reference	4	Places

[a]The ultrasonic flowmeter was not connected to the data acquisition for initial operation.
[b]One set of salt level probes available for use in a test port were not used during initial operation.

1.1 ADDITIONAL DESIGN INFORMATION

1.1.1 Main Heater Thermocouples

The main heater includes 48 thermocouples recessed into grooves on the outside faces of the plate. These thermocouple locations are depicted in Figure 3 and Figure 4. Note that these figures are oriented as direct views of the surface. For example, the top right quadrant is grid *B* relative to a viewer looking at the front face of the plate, whereas the top right quadrant is grid *F* relative to a viewer looking at the back face. In actuality, grid *F* thermocouples are on the plate surface behind grid *A*. The heater plate geometry was designed such that there is front-back and left-right symmetry. This symmetry was accounted for when the thermocouple locations were chosen to limit overlap.

As noted in the design report [4], trace heating was applied to the front and back faces of the main heater. This trace heating was in the form of heat tapes applied in a serpentine shape without symmetry. Also, some thermocouples may reside under the heat tapes and others in the gaps of the serpentine arrangement of the heaters. With the heaters on, thermocouples under the heat tapes are expected to be at higher temperatures than the thermocouples not under the heat tapes. Altogether, trace heating is expected to cause some temperature variations in thermocouple data, despite the plate's geometric symmetry.

During the first operation, five thermocouples (TC numbers 30, 37, 40, 44, and 47) were disconnected. The heat trace on the face of the main heater was controlled using four thermocouples (TC numbers 3, 15, 31, and 46).

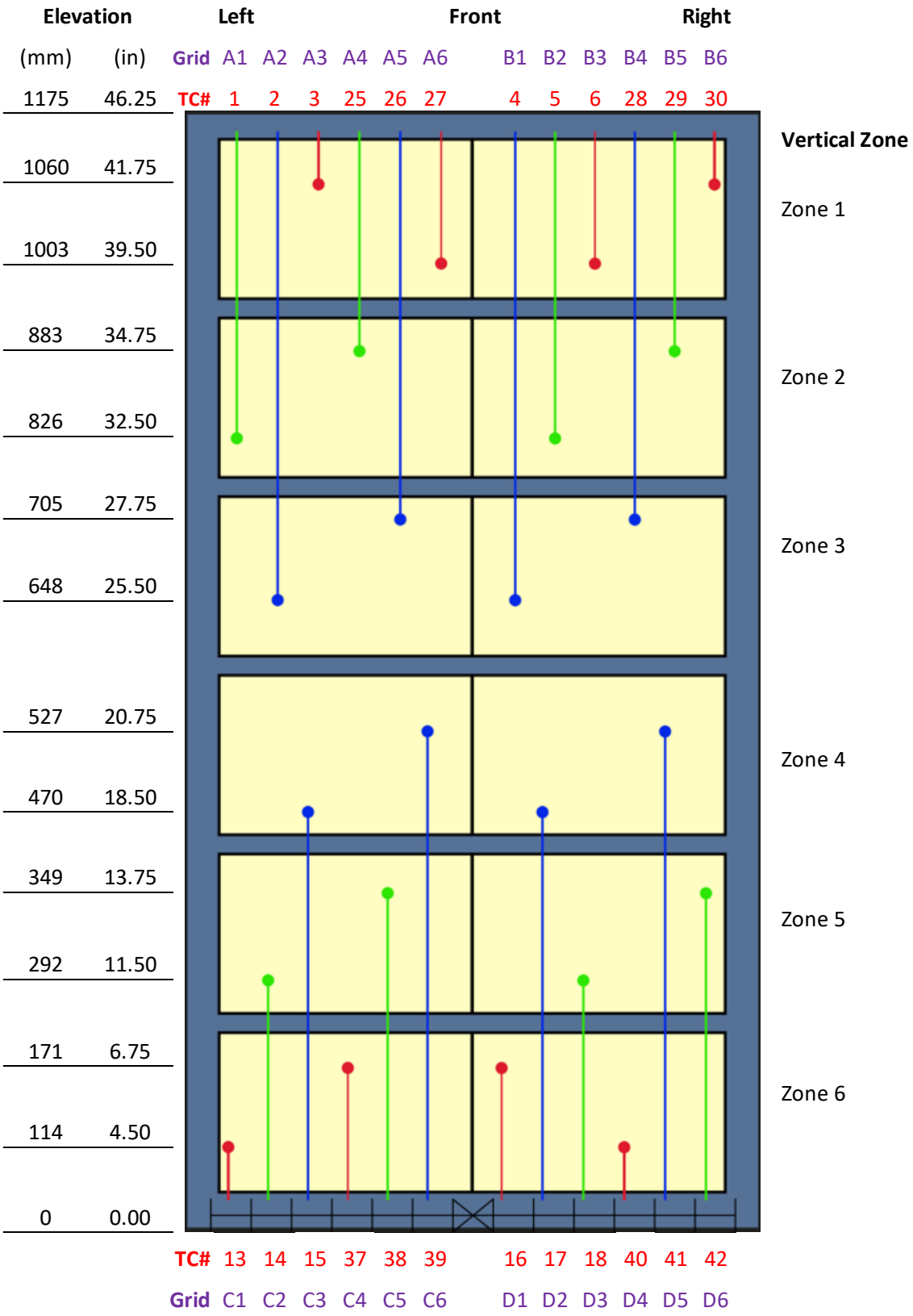

Figure 3. Thermocouple locations on front face of the main heater.

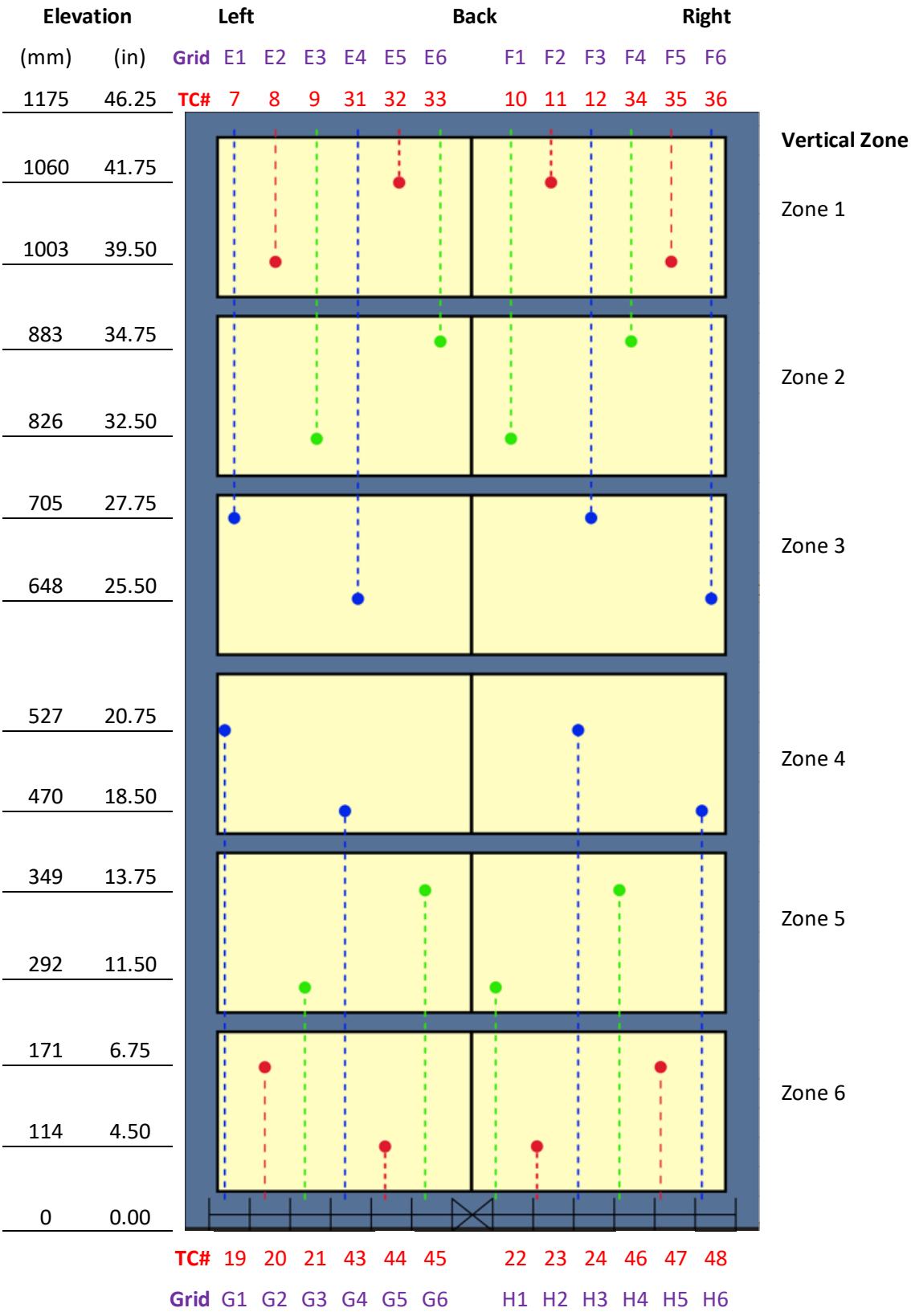

Figure 4. Thermocouple locations on back face of the main heater.

1.1.2 Heat Exchanger Thermocouples

To monitor temperatures, 11 thermocouples were fastened with tack-welded metal strips onto the outside surfaces of the heat exchanger's finned tubes. However, the difficulties of attaching the thermocouples to the finned tube geometry resulted in non-ideal thermal contact which adds uncertainty to the interpretation of the measured temperatures.

The thermocouples are grouped into three zones: upper, middle, and lower. The upper zone is approximately 6.2 in. below the top tube manifold and contains two thermocouples. The middle zone is near the middle of the finned tubes and contains three thermocouples. Finally, the lower zone is 4.1–5.8 in. above the bottom tube manifold and contains six thermocouples. Looking at the front face of the heat exchanger, the tubes in the front row are numbered 1–8 from left to right. During blower operation, the air first impinges this row of tubes. Tubes numbered 9–16 from left to right are staggered behind the front tubes. For the first operation, temperature data were monitored and recorded for 10 of the 11 thermocouples. The thermocouple locations are 4U, 3M, 6M, 11M, 1L, 2L, 5L, 7L, 8L, and 14L, where the number is the tube number, and the letters correspond to the upper (U), middle (M), and lower (L) zones. The thermocouple locations are illustrated in Figure 5.

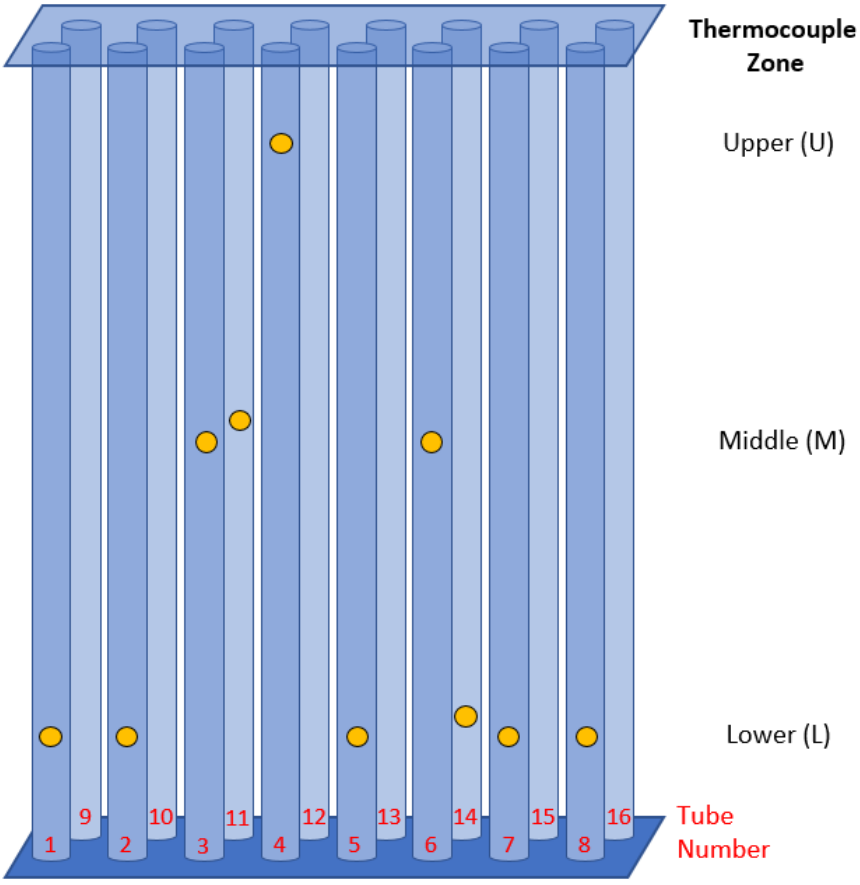

Figure 5. Illustration of heat exchanger thermocouple locations.

1.1.3 Gas Pressure Transducers

The gas space pressures were measured using Honeywell PF2000 pressure transducers with a listed 0.10% accuracy.

2. SHAKEDOWN OPERATIONS

2.1 PUMP WATER TESTING

2.1.1 Manufacturer Testing

As part of the acceptance testing in late 2020, the pump manufacturer ran a series of tests on the pump using water in an open pit (i.e., at room temperature and pressure). Three pump curves were developed as shown in Figure 6. The water testing was consistent with pre-test predictions except for slightly higher than anticipated shutoff heads at zero flow rate, as seen in Figure 6. The pump is designed to run at shutoff conditions for short periods. Operation at shutoff conditions was demonstrated at four speeds: 500, 1,050, 1,200, and 1,800 rpm. In addition to the pump curve testing, the pump's displacement due to vibration was measured and the bearings and seal were thermally imaged during operation.

The shaft seal was damaged during water testing with the mini-loop at ORNL (see Section 2.1.2). The cause was traced to incomplete installation. The pump was returned to the manufacturer, and the seal was refurbished in early 2022. The manufacturer tested the refurbished pump in water at 500, 1,050, 1,200, and 1,800 rpm for 15 min each. During this hour of operation, the temperatures of the seal, thrust and radial bearing, and motor were monitored as well as pump vibration. Inspection of the seal after these operations demonstrated the system worked as designed.

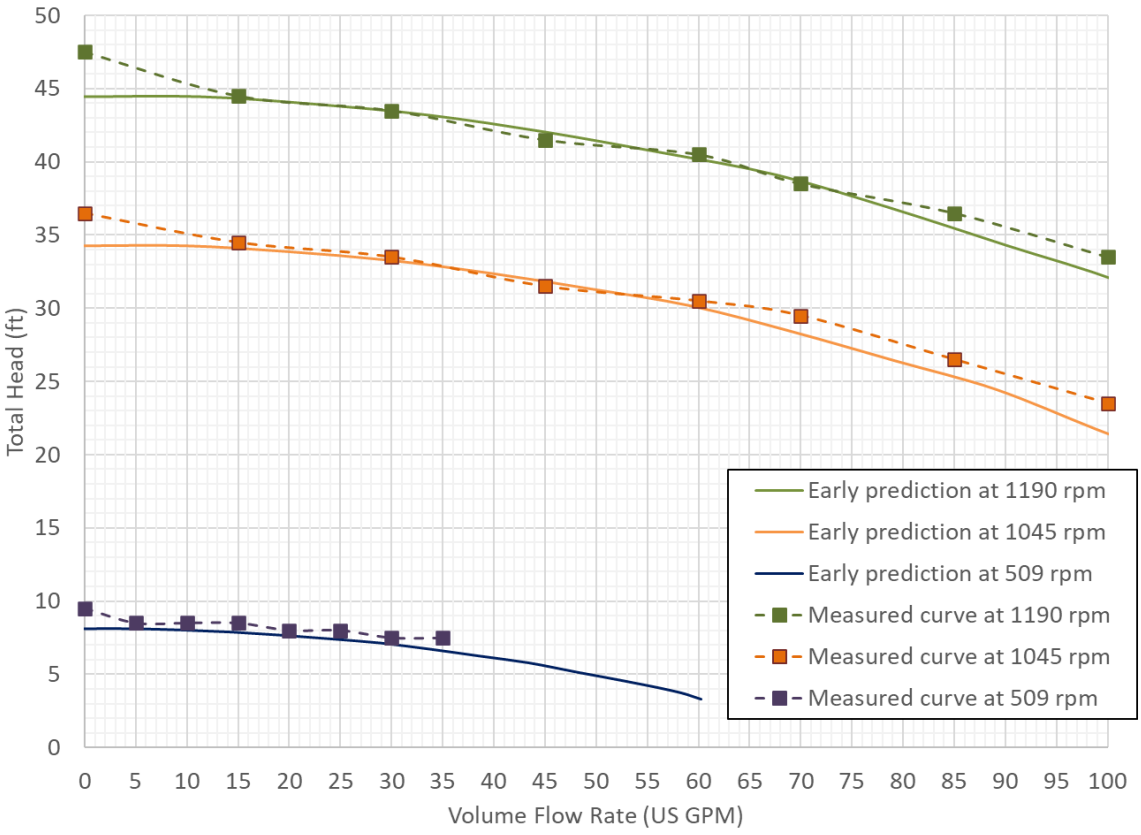

Figure 6. Measured and anticipated pump head curves with water.

2.1.2 Mini-Loop Tests

While waiting for the other components to complete the flow loop, the pump was installed in the pump tank. A temporary loop was constructed in late 2021 with plastic piping to test the installed pump. This "mini-loop" started at the pump discharge, raised vertically, passed over the pump motor, and then returned to the pump tank inlet. Instrumentation included two flowmeters and a pressure transducer. A gate valve located near the pump tank inlet was used to vary the loop's pressure drop. A clear section within the mini-loop provided a means to visually check for gas entrainment.

The pump curves from the testing are shown in Figure 7 and compared against those measured by the manufacturer. The pump curves follow the expected trends. No noticeable gas entrainment occurred under any of the flow and pump speed conditions tested.

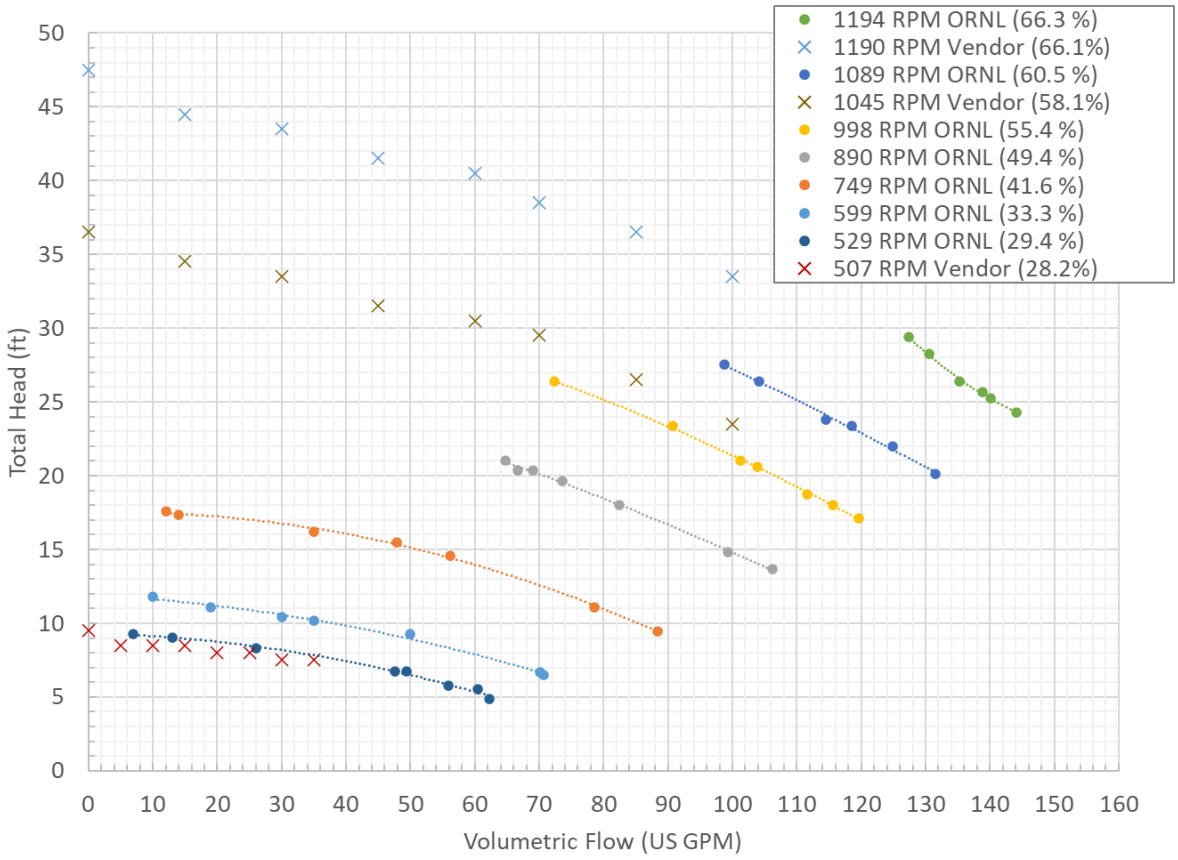

Figure 7. Pump curve water test data.

The ORNL data at 749 rpm were correlated with a quadratic function with an R^2 of 0.9976. This correlation was translated to the speeds tested by the manufacturer using the using the pump affinity laws shown in Eq. (1) and Eq. (2), where H is the pump head, N is the impeller frequency, and Q is the volumetric flow rate. There is good agreement between the translated correlation and the manufacturer's data, as shown in Figure 8. The mini-loop water testing provides independent verification of the pump curves supplied by the vendor.

$$\frac{H_1}{H_2} = \frac{N_1}{N_2} \tag{1}$$

$$\frac{Q_1}{Q_2} = \left(\frac{N_1}{N_2}\right)^2 \tag{2}$$

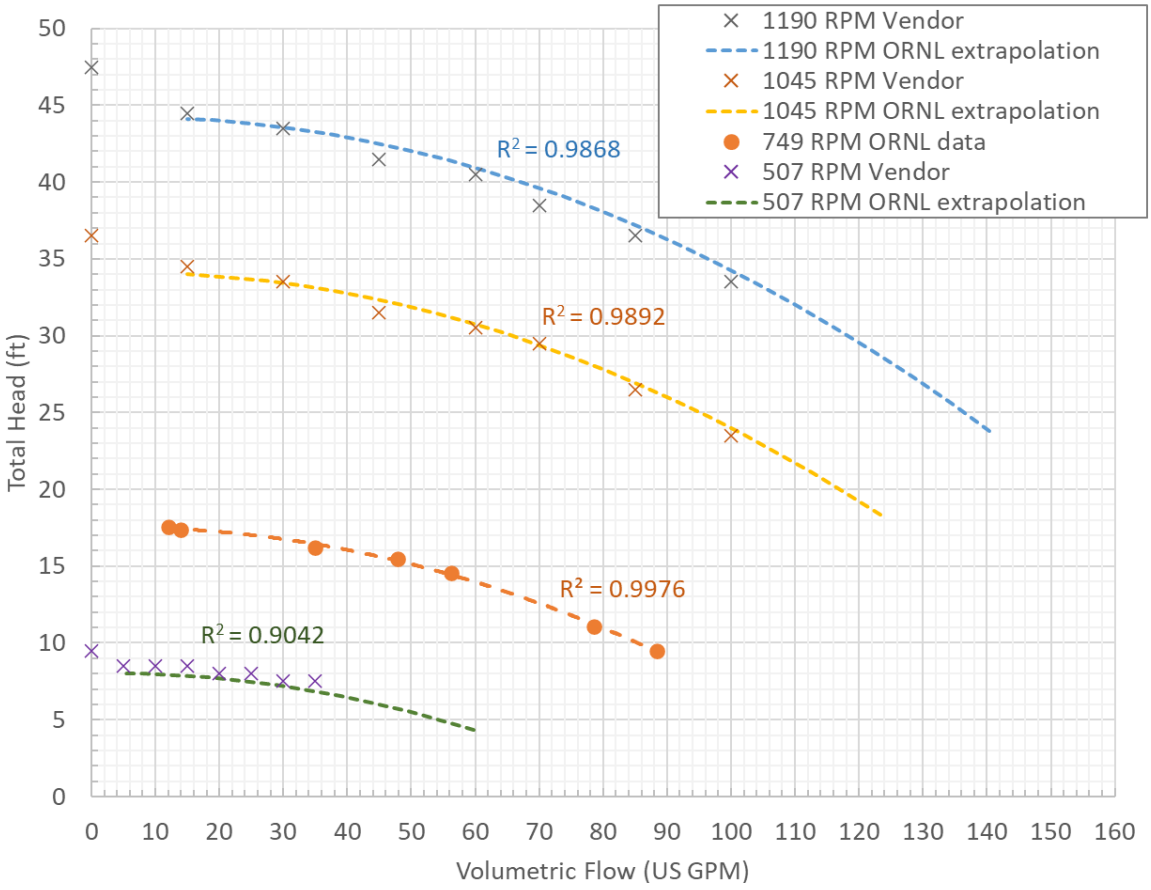

Figure 8. Vendor pump curves compared with correlation extrapolated from 749 rpm ORNL data.

2.1.3 Full-Loop Tests and Comparison with Prediction Results

After the refurbished pump was received (see Section 2.1.1), it was installed in the pump tank at ORNL in May 2022, thus completing the forced-flow loop circuit. Water was pneumatically raised into the loop, and the pump was operated at a variety of speeds to confirm shaft seal and overall pump performance. Because the primary goal of the testing was to confirm shaft seal operation, flow measurements were not taken. The pump speed and the pressures in the pump tank and top port were recorded as shown in Table 3. The testing was conducted at room temperature, and the liquid level in the top port was maintained to within ± 0.8 in. (i.e., ± 0.07 ft head of water).

Table 3. Full-loop water test data.

Pump speed nominal (%)	Pump speed actual (%)	Pump speed (rpm)	Top port gas pressure *P2* (psig)	Pump tank gas pressure *P1* (psig)	Gas pressure difference *P4 = P1 − P2* (psi)	Flow loss *P5 = P4 − P3* (psi)	(ft)
0	0.0	0.0	3.45	12.01	8.56 (P3)	0	0
33	32.4	583.4	4.60	12.70	8.10	0.46	1.06
35	34.4	619.4	4.60	12.61	8.01	0.55	1.28
40	39.4	709.5	4.60	12.50	7.89	0.67	1.54
42	41.4	745.5	4.60	12.43	7.82	0.74	1.70
45	44.4	799.5	4.60	12.33	7.73	0.83	1.91
50	49.4	889.6	4.53	12.04	7.50	1.06	2.45
50	49.4	889.6	4.37	11.85	7.48	1.08	2.50
50	49.4	889.6	4.60	12.08	7.48	1.08	2.50
50	49.4	889.6	4.60	12.08	7.48	1.08	2.50
55	54.4	979.7	4.60	11.92	7.32	1.24	2.87
55	54.4	979.7	4.60	11.92	7.32	1.24	2.87
60	59.4	1,069.8	4.60	11.64	7.04	1.52	3.51
60	59.4	1,069.8	4.60	11.64	7.04	1.52	3.51
65	64.4	1,159.8	4.60	11.41	6.81	1.75	4.04
70	69.4	1,249.9	4.60	11.16	6.56	2.00	4.62

The head form of the isothermal steady flow energy equation between points in the loop is provided in Eq. (3), where P is pressure, ρ is the fluid density, g is gravity, V is the fluid velocity, z is the relative height, h_{pump} is the head added by the pump, and $h_{flow\ loss}$ is the head flow loss. The head flow loss is the sum of the loss caused by friction, $h_{friction}$, and the loss caused by viscous effects in flow geometry changes, $h_{minor\ loss}$, as shown in Eq. (4). When the stagnant gas space in the top port is chosen for the inlet point, and the stagnant gas space in the pump tank is chosen for the outlet point, Eq. (3) reduces to Eq. (5).

$$\left(\frac{P}{\rho \cdot g} + \frac{\alpha}{2 \cdot g} V^2 + z\right)_{in} = \left(\frac{P}{\rho \cdot g} + \frac{\alpha}{2 \cdot g} V^2 + z\right)_{out} - h_{pump} + h_{flow\ loss} \tag{3}$$

$$h_{flow\ loss} = h_{friction} + h_{minor\ loss} \tag{4}$$

$$\left(\frac{P}{\rho \cdot g} + z\right)_{in} = \left(\frac{P}{\rho \cdot g} + z\right)_{out} - h_{pump} + h_{flow\ loss} \tag{5}$$

When the pump is not operating and negligible flow in the loop is assumed, Eq. (5) further simplifies to Eq. (6). The term on the right of Eq. (6), the change in static head, can be determined using the measured pressures at the inlet and outlet and the salt density. During pump operation, if the salt temperature and liquid levels do not vary, then the static head term does not change.

$$\left(\frac{P}{\rho \cdot g_{out}} - \frac{P}{\rho \cdot g_{in}}\right) = (z_{in} - z_{out}) \tag{6}$$

In the return side of the loop (i.e., the flow path between the top port and the pump tank on the left side of Figure 1), the flow does not pass through the pump. Therefore, Eq. (5) can be simplified to Eq. (7), in

which the total head flow loss through the return side of the loop can be determined during operation using the pressure measurements at the top port and pump tank and the static head determined during nonflowing operations.

$$h_{flow\ loss} = \left(\frac{P}{\rho \cdot g}_{out} - \frac{P}{\rho \cdot g}_{in}\right) - (z_{in} - z_{out}) \quad (7)$$

The gas pressure differences (denoted as *P4*) between the measured pump tank gas space and the top port gas space were calculated and are provided in Table 3. When the fluid is not flowing (i.e., zero pump speed), *P4* is a measure of the static head differential between the two gas space measurements, as shown in Eq. (6). This static head is denoted as *P3* in Table 3. The flowing salt experiences pressure losses caused by friction and geometric effects such as bends, expansions, and contractions. The fluid pressurization from the pump offsets the flow losses. Because the fluid levels were maintained constant during pump operation (i.e., the static head did not change), the flow losses on the return side of the loop can be calculated using Eq. (7). The calculated flow losses for the return side, denoted as *P5*, are provided in the two rightmost columns of Table 3 in units of psig (pressure) and feet (head).

Expected flow losses can be estimated for comparison with the measured data. Estimating these losses requires engineering correlations for the minor and frictional losses in Eq. (4). The minor flow losses can be estimated using Eq. (8), where *K* is a geometry-dependent flow loss coefficient, and *V* is the fluid velocity. A flow loss coefficient of 1.4 was assigned for combined contraction and expansion losses (e.g., the flow contraction into and the expansion out of the main heater) [5]. A flow loss coefficient of 0.19 was assigned for the combined pipe bends near the wye sections of piping. The other pipe bends were also assigned a flow loss coefficient of 0.19. The head loss resulting from friction effects can be estimated using Eq. (9), where *L*, *D*, and *V* are the length, inner diameter, and fluid velocity, respectively, of each piping segment. The friction factor, *f*, was calculated using the Blasius correlation for turbulent flow as shown in Eq. (10). The Reynolds number, *Re*, is dependent on the fluid density, ρ, and viscosity, μ, as shown in Eq. (11). The salt density and viscosity properties assumed based on Zhao are given in Table 4 [6].

$$h_{minor\ loss} = \frac{1}{2g}\sum(K \cdot V^2) \quad (8)$$

$$h_{friction} = \frac{1}{2g}\sum\left(\frac{f \cdot L}{D} \cdot V^2\right) \quad (9)$$

$$f = 0.316\, Re^{-1/4} \quad (10)$$

$$Re = \frac{\rho \cdot V \cdot D}{\mu} \quad (11)$$

Table 4. Assumed salt properties.

	560°C	**700°C**
Viscosity (Pa·s)	0.0030	0.0024
Density (kg/m^3)	1,642	1,561

With these assumptions, the total head flow losses around the loop were estimated for water at 25°C, salt at 560°C, and salt at 700°C as functions of flow rate. In addition to the total flow losses for the loop, the losses for the supply side (from pump tank to top port) and the return side (from top port to pump tank) were individually calculated. These estimated head flow losses are shown in Figure 9–Figure 11.

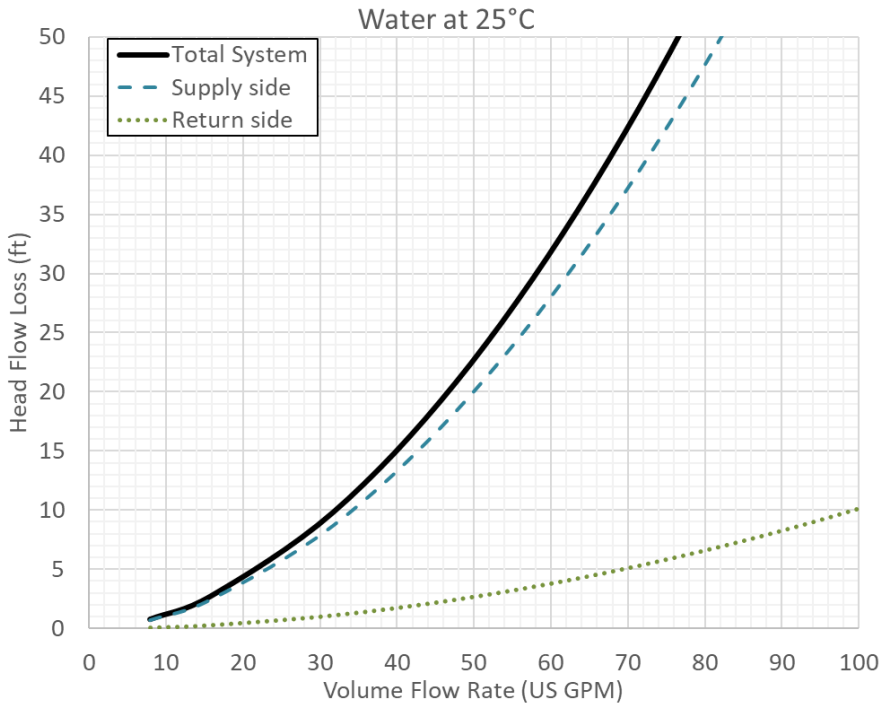

Figure 9. Predicted head flow losses around the loop for water at 25°C.

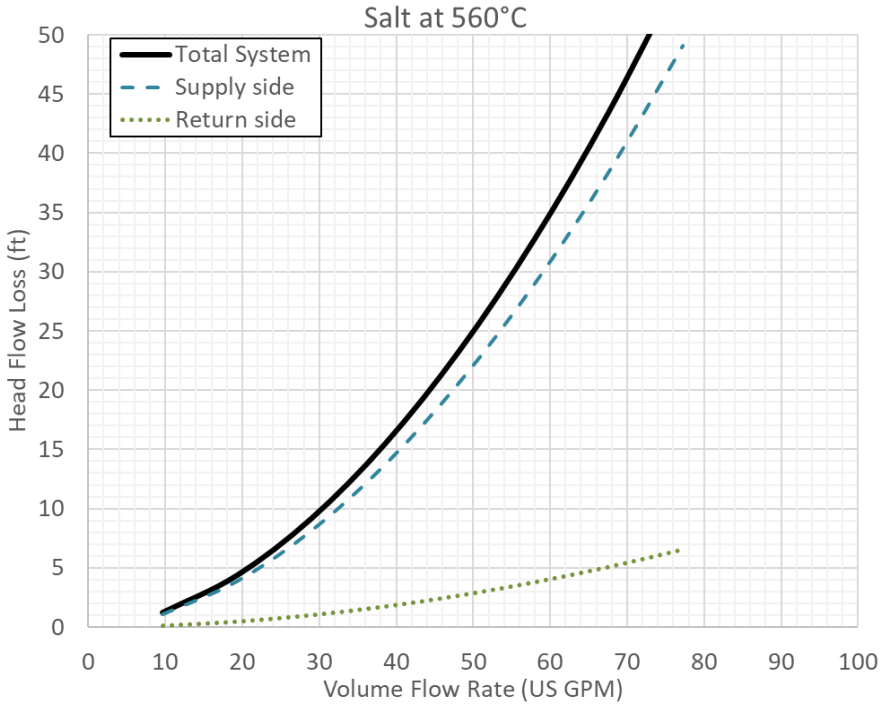

Figure 10. Predicted head flow losses around the loop for salt at 560°C.

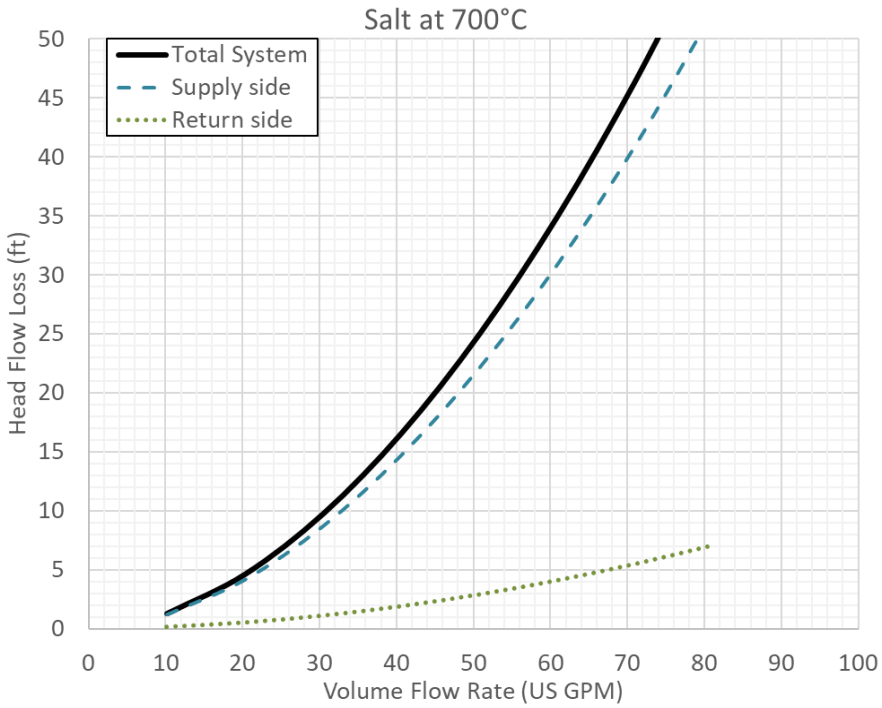

Figure 11. Predicted head flow losses around the loop for salt at 700°C

The total head flow losses as functions of flow rate (i.e., system curves) are plotted with the pump curves in Figure 12. During operation at a specified pump speed, the intercept between the appropriate system curve and the pump curve is the flow rate and system total head. These intercept points as a function of pump speed were extracted and are provided in Figure 13 for the water system, in Figure 14 for the salt system at 560°C, and Figure 15 for the salt system at 700°C.

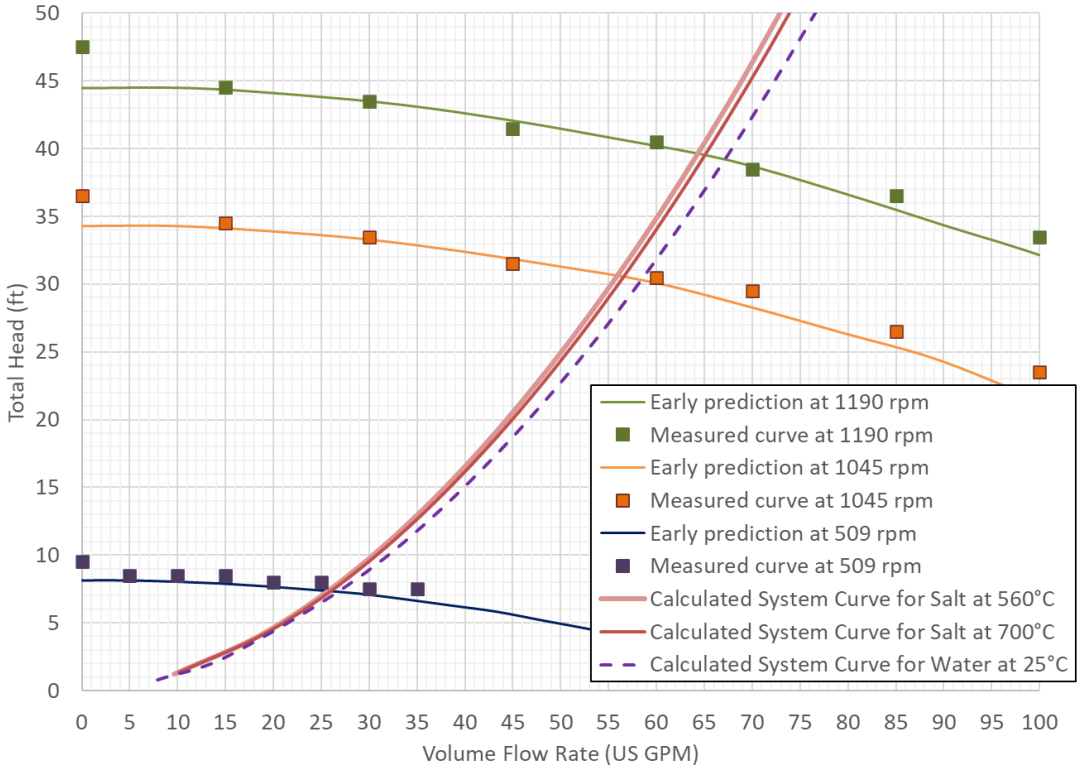

Figure 12. Pump curves with predicted system curves.

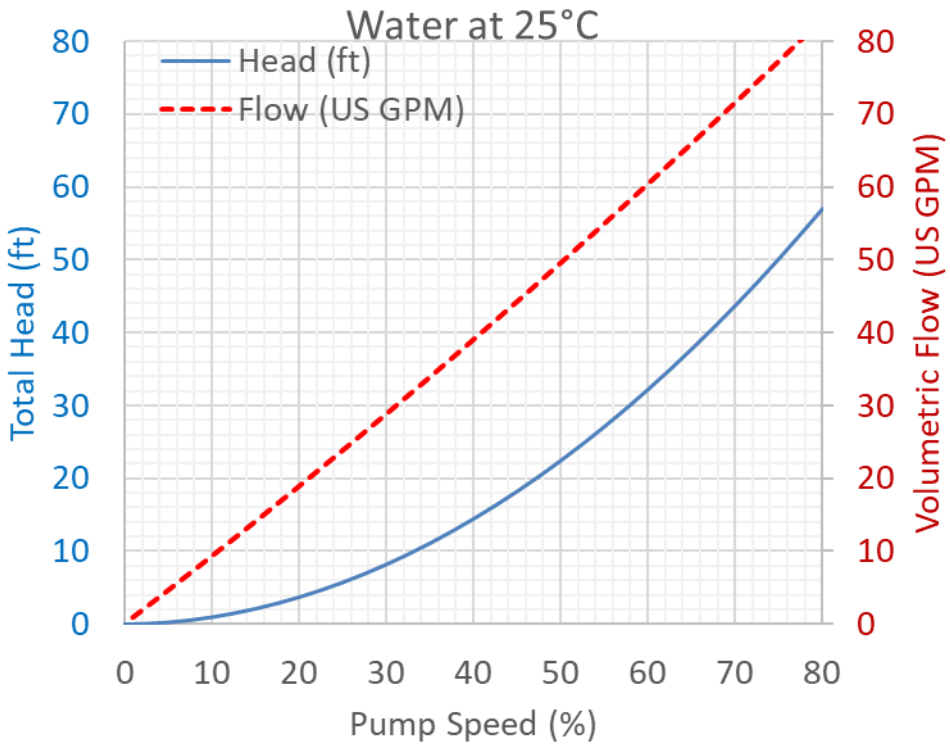

Figure 13. Predicted total head and flow rate as functions of pump speed for water at 25°C.

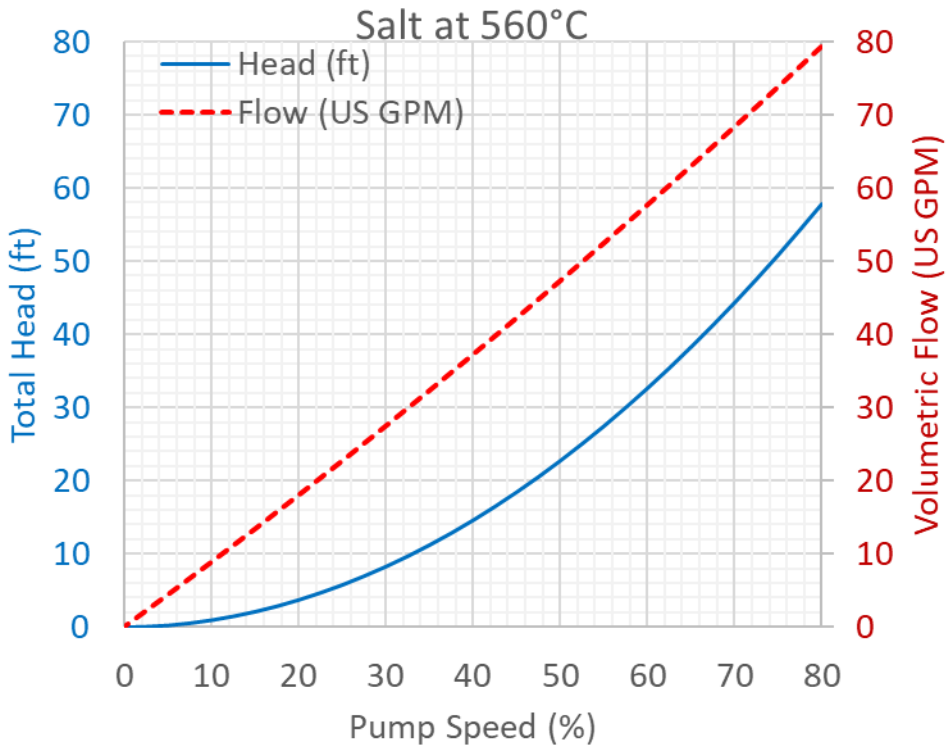

Figure 14. Predicted total head and flow rate as functions of pump speed for salt at 560°C.

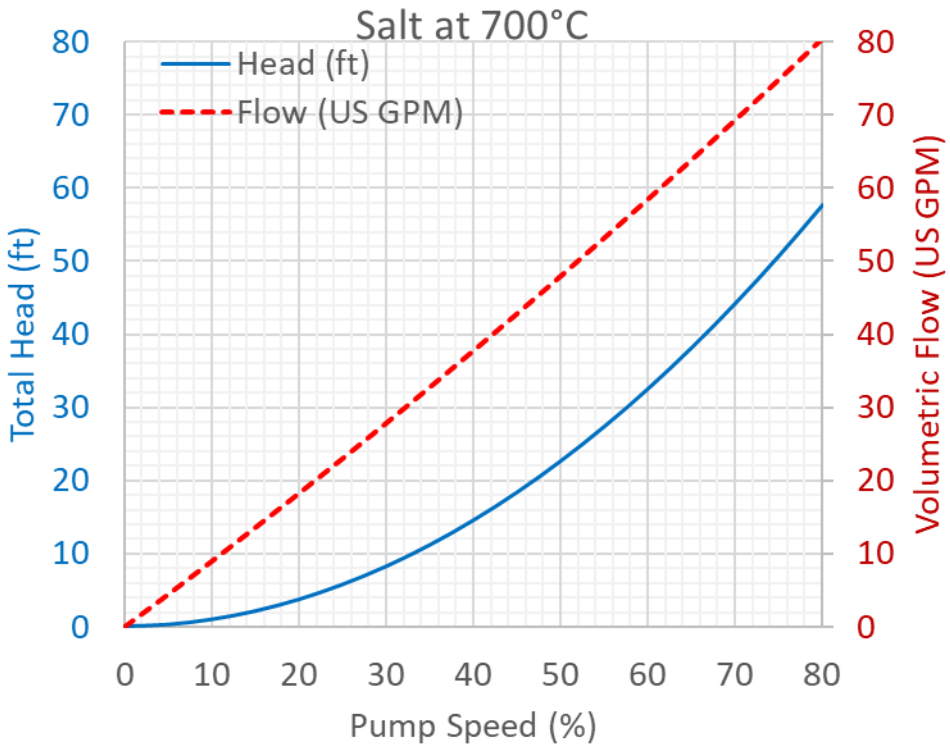

Figure 15. Predicted total head and flow rate as functions of pump speed for salt at 700°C.

The flow loop conditions during operation can be determined from Figure 9 through Figure 15. For example, at a specified pump speed with the system filled with water, the predicted system flow rate can be determined using data provided in Figure 13. For that predicted system flow rate, the predicted head loss in the return side of the loop can be estimated using data presented in Figure 9. This process was performed for the water test data from Table 3. Figure 16 compares the predicted head flow loss for the return side of the loop with the measured data. The agreement is surprisingly good given the simple flow loss modeling used for the predictions; the predicted flow loss is approximately 8% higher than the measured data. This favorable result provides some confidence and validation of the predicted system characteristics. Future refinements to the modeling may improve agreement.

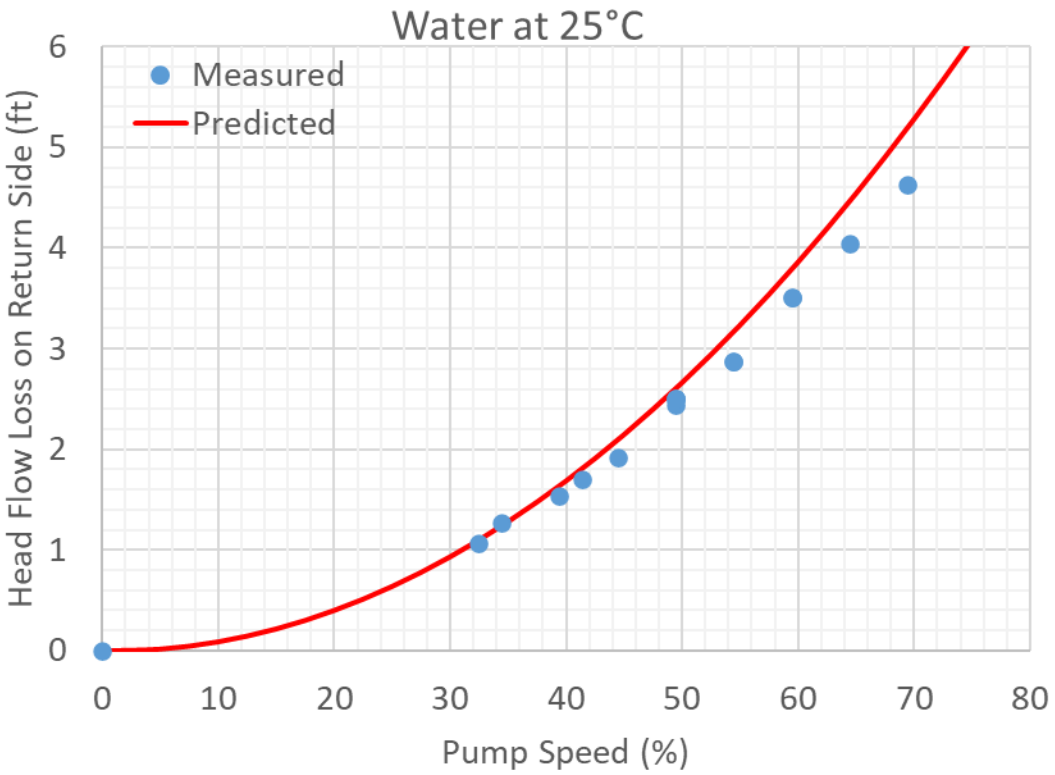

Figure 16. Comparison of the predicted and measured head flow loss in the return side of the loop for the water test data.

2.2 ISOTHERMAL HEATING CHARACTERISTICS

2.2.1 Trace Heat Isothermal Losses

In preparation for initial operation, the flow loop was incrementally heated while filled with Ar. The duty cycle for each heater zone was recorded at various temperature hold points. The time-averaged power for each zone was calculated based on the heater's nominal design power, supplied voltage, and duty cycle, thus providing an estimate of the power required for each zone to offset the isothermal heat losses at various set temperatures. As installed and operated, the usable loop trace heating capacity is 71,400 W, 30,200 W of which is for the heat exchanger auxiliary heaters.

The isothermal heat losses for each zone can be used in future modeling of the system to inform future analysis and interpretation of test data (e.g., heat transfer tests). The trace heating requirements depend on particulars of the heater arrangement, insulation, and component mounting. Thus, the isothermal heat

losses from FASTR are unique to the facility. However, the information discussed in the remainder of this subsection may also inform the trace heating requirements for similar, future facilities.

The heat exchanger dominated the trace heating requirements. Tubular heaters are mounted to the inlet and outlet plenums of the heat exchanger, forming two independently controlled heater zones, a top plenum zone and a bottom plenum zone. Offset slightly away from the finned tubes, serpentine tubular heaters cover the front and back faces of the heat exchanger and are grouped into two independently controlled zones, a top-face zone and a bottom-face zone. The heat exchanger core and four heater zones reside within an insulated enclosure formed by raising two insulated doors to cover the air inlet and outlet to the heat exchanger. An outer stainless steel (SS) duct contains and directs the air flow across the heat exchanger. Additional heaters called *auxiliary heaters* were added to the air duct near the insulated doors.

The heat losses for the flow loop, excluding the storage tank and the transfer line between the storage tank and pump tank, are illustrated in Figure 17 as a function of nominal setpoint. The heat exchanger accounted for a substantial fraction of the trace heating requirements. Maintaining the system at a nominal 565°C requires approximately 27,800 W (i.e., 39% of total installed capacity). As shown in Figure 18, the heat exchanger requires 10,900 W (4,000 W core and 6,900 W auxiliary), accounting for approximately 46% of the required trace heating. The isothermal heat loss trends for the main heater, pump tank, and storage tank are shown in Figure 19.

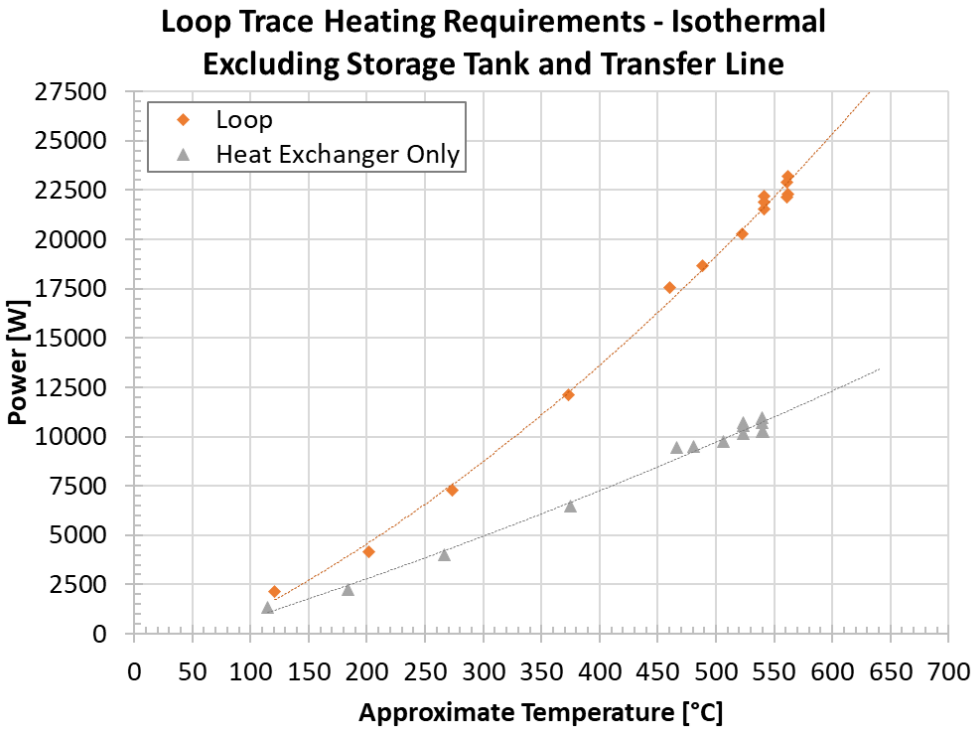

Figure 17. Loop isothermal trace heating requirements.

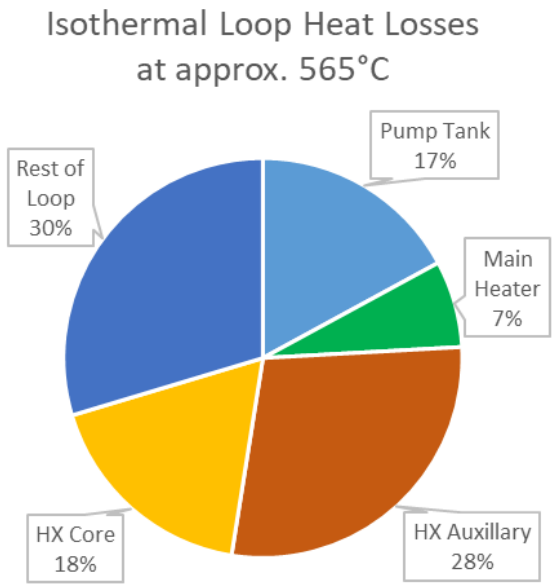

Figure 18. Summary of heat losses at approximately 565°C.

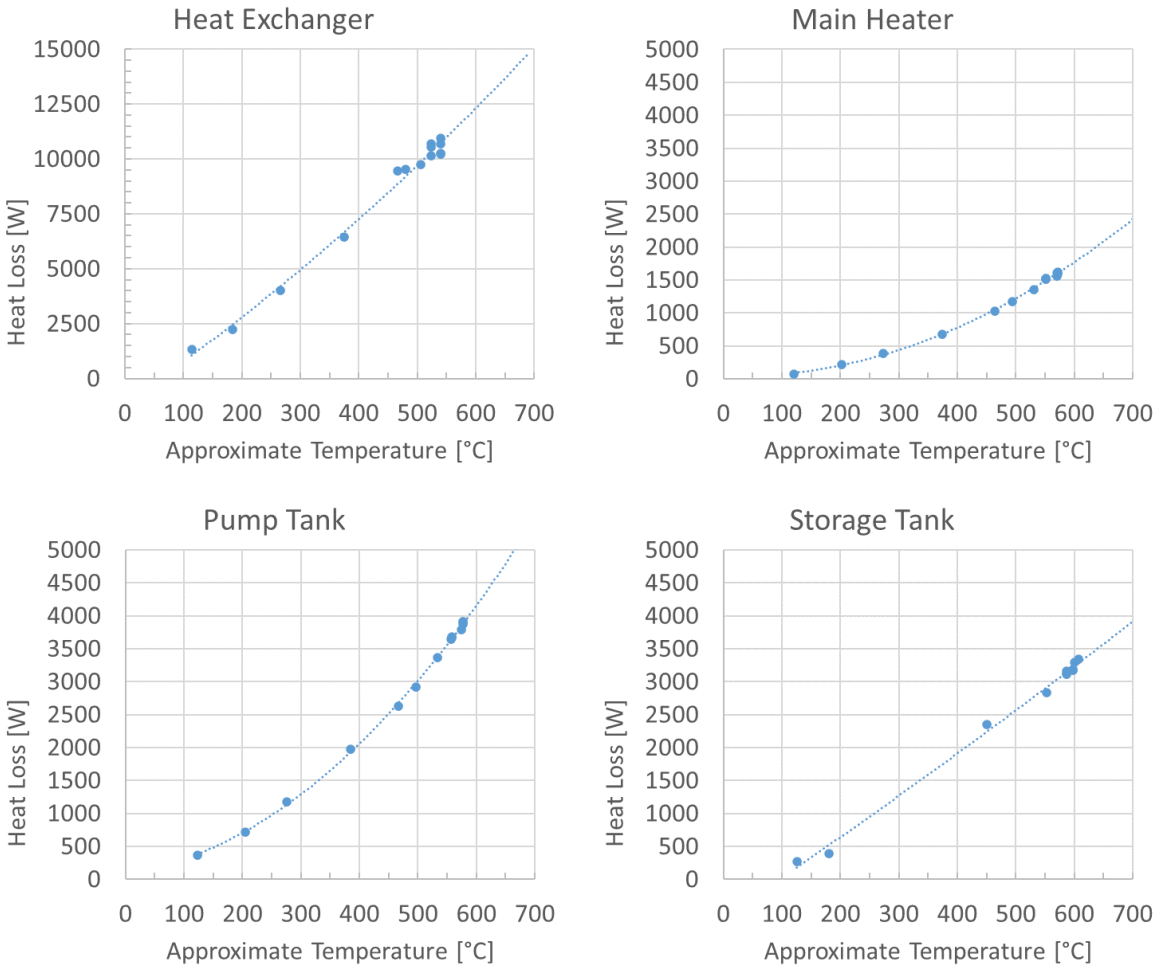

Figure 19. Individual component isothermal heat losses.

2.2.2 Thermal Imaging

Thermal images of the system were taken when the loop was preheated to approximately 560°C. Examples of these images are shown in Figure 20. The exposed system materials (e.g., smooth or embossed aluminum sheathing around insulation, oxide insulation, and metal alloys) have a range of emissivities. The images were not corrected for the differences in emissivities and therefore are not quantitative measurements.

The thermal images may be used to identify changes in the system's thermal characteristics. Analysis of the images revealed locations requiring additional insulation (e.g., gaps in insulation, insufficient thickness). These baseline images can be compared with future thermal imaging to identify failures of trace heating segments or changes in insulation performance.

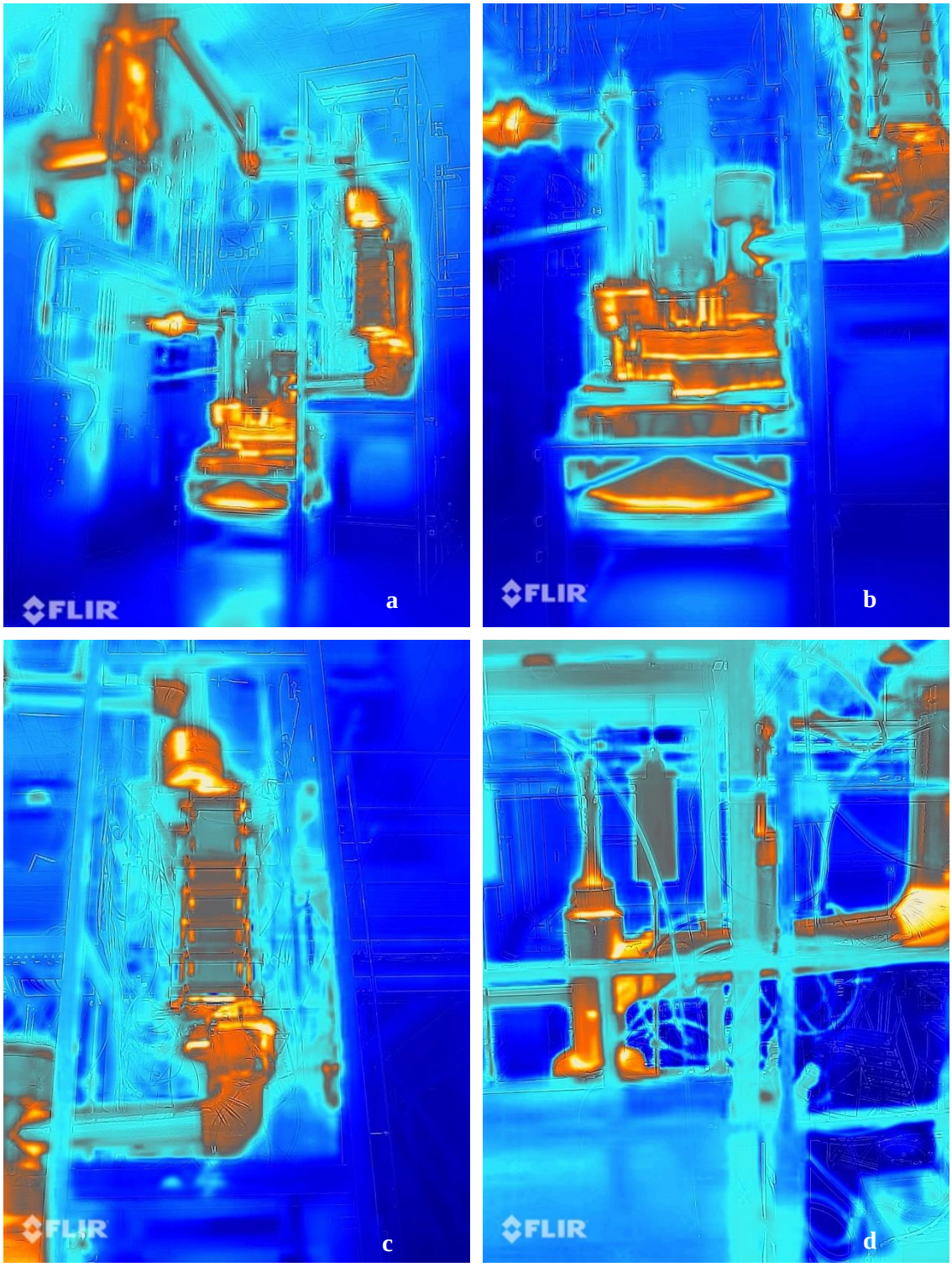

Figure 20. Example thermal images of the (a) overall system, (b) pump and pump tank, (c) main heater, and (d) top piping.

2.3 OTHER ACTIONS AND COMMENTS

Additional activities were completed in support of loop commissioning. The system was leak checked via a pressurization decay curve method, and individual locations were checked via a handheld gas detector. Both activities were performed at room and elevated temperatures. System alarms and trips set in the programmable logic controller (PLC) were verified to the extent possible, as were instrumentation and control (I&C) signals (e.g., temperature, flow, pressure) and their mapping in the PLC. The pump was operated dry before the water testing to check for rotation direction, vibration, and shaft seal gas consumption and temperature. This dry testing was conducted at room and elevated temperatures. After water operations, the loop was dried through a combination of heating and long-term dehumidification by flowing dry Ar through the system.

3. SALT OPERATION

3.1 SALT ADDITION

After purification, the salt is stored in the storage tank and allowed to freeze. In preparation for transferring the salt to the loop, it was melted within the storage tank, and the remainder of the facility was preheated to a nominal 565°C. Before pumped operation, the loop is prefilled with salt pneumatically by controlling the flow and pressure of the Ar ullage gas in the storage tank, pump tank, and top port of the loop. The salt is transferred from the storage tank to the pump tank and then pneumatically raised into the flow loop, filling the system up to the top port.

During the initial filling of the loop for this effort, it was discovered there was insufficient salt to fill the loop completely while maintaining the required salt level above the pump suction inlet. The deficit was estimated to be approximately 20 L. Multiple factors leading to this salt deficit largely stemmed from the parallel design, revision, and fabrication of the loop hardware. Examples include the redesign of the heat exchanger necessitated by supply chain limitations, the initially undefined minimum required salt depth for the pump, and a shortage of available salt for the initial purification process. To address the deficit, an additional 59.6 kg (approximately 36 L) of salt was purified and added to the system, bringing the total salt mass in the system to 253.7 kg.

3.1.1 Second Purification Process

The purification system described by Robb et al. [3] was used to purify the additional required salt. The second purification operation largely mirrored the first [3]. However, there were several notable differences between the purification operations for the first and second batches. These differences are summarized in Table 5 and described in this subsection.

The batch of additional salt was approximately a quarter of the size of the first batch. Because the availability of salt was limited, a blend of anhydrous carnalite from Israel Chemicals Ltd. (ICL) and pure constituent salts from chemical suppliers were used. Table 6 summarizes the salt loaded into the vessel, a 58.9 kg blend that is approximately 43.4 $MgCl_2$–37.1 KCl–19.5 NaCl (wt %).

The scrubber for the second purification operation used a caustic KOH solution in the first and second stages. This reduced the hazards associated with handling very low-pH acid.

Goals for the first purification operation included purifying the salt, as well as methodically instrumenting and conducting the process to capture data to inform future processes. The goal of the second operation was to purify salt to rectify the insufficient salt volume for loop operation. The RGA, electrochemical probe, and scrubber pH sensor were not used in the second operation because of the limited time, batch size, and the use of a caustic solution. The humidity sensor was also not used because it failed during the first operation.

Table 5. Comparison of first and second salt purification operations

Process parameter	First batch	Second batch
Salt mass loaded in purification vessel	212.2 kg	58.94 kg
Salt mass transferred to storage tank	194.1 kg	59.6 kg
Total time **Low-temperature hold** **High-temperature hold**	20 days 7 days total, 250 and 300°C 10 days total, 500°C–675°C	7 days 1.7 days, 250°C 4.0 days, 565°C
Initial scrubber contents[a] **Vacuum** **1st scrubber** **2nd scrubber** **3rd scrubber**	 1,003 g H_2O 2,002 g H_2O 1,501 g H_2O 1,516 g H_2O	 10 wt % KOH in 2,003 g H_2O 5 wt % KOH in 2,001 g H_2O 2,000 g H_2O 1,501 g H_2O
Mg addition total **Initially loaded** **Added during process** **Mg form**	484 g 241 g 243 g Primarily chips	101.1 g 11.8 g 89.3 g Rods
Total line plugging events **Effluent line plugging events** **Bubbler line plugging events**	4 1 3	0 0 0
Bubbler line end geometry	45° cut	90° cut
Filters during transfer	3 filters (40, 25, and 5 μm)	1 filter (25 μm)

[a]reflects initial scrubber contents during setup; water was demineralized (18 MΩ).

Table 6. Salt added into purification vessel

Main constituents	Description	Mass (kg)
$MgCl_2$, KCl, NaCl	Anhydrous carnalite, ICL	38.36
KCl	≥99.5% (argentometric), Merck KGaA	6.86
$MgCl_2$	≥98% anhydrous, Sigma-Aldrich	7.72
NaCl	≥99.5% (AT), Sigma-Aldrich	6.00
Total	—	58.94

The second operation was accelerated compared to the first. The durations of the low- and high-temperature holds were both reduced. The low-temperature hold at 250°C was approximately half the duration of the first process duration: 1.7 days compared to 3.2 days. During the first operation, water release was largely completed during the 250°C hold. Because the second operation purified approximately 72% less salt than the first operation, a duration of 1.7 days for the 250°C hold was judged to be sufficient. During the first operation, very little water was released during the 300°C hold. Therefore, the hold at 300°C was not performed during the second operation. For the high-temperature hold during the second operation, the salt was held at 565°C instead of the 500°C–675°C range used during the first operation. The salt was not heated above the melting point of Mg (650°C) during the second operation because the measurements taken during the first process did not show a clear benefit of doing so.

Notably, the effluent line and the bubbler tube did not plug during the second operation, in which the bubbler line was replaced with a new tube terminating in a flat 90° cut instead of a 45° angle. Other

factors that may have contributed to the line not plugging during the second operation were (1) the reduced salt batch weight, which resulted in a lower hydrostatic head of salt, (2) optimized gas flow rates, and (3) a higher processing temperature of 565°C instead of 500°C and 550°C.

For the second purification, much less Mg was initially loaded with the salt. It is suspected that a substantial fraction of the initial Mg chips added for the first purification was oxidized during the low-temperature dehydration of the salt. For the second operation, the Mg was added in the form of rods. The timing of the Mg additions during the high-temperature hold is plotted in Figure 21. Each of the 15 additions was 5.8–6.0 g. Because the rods have less surface area than the chips, less MgO was introduced during Mg addition; the reduced surface area may also slow the reaction rate with the salt, thus reducing the rate of H_2 generation. The rod form is also easier to handle and introduce into the purification vessel. All these effects are advantageous and motivated the use of Mg in rod form.

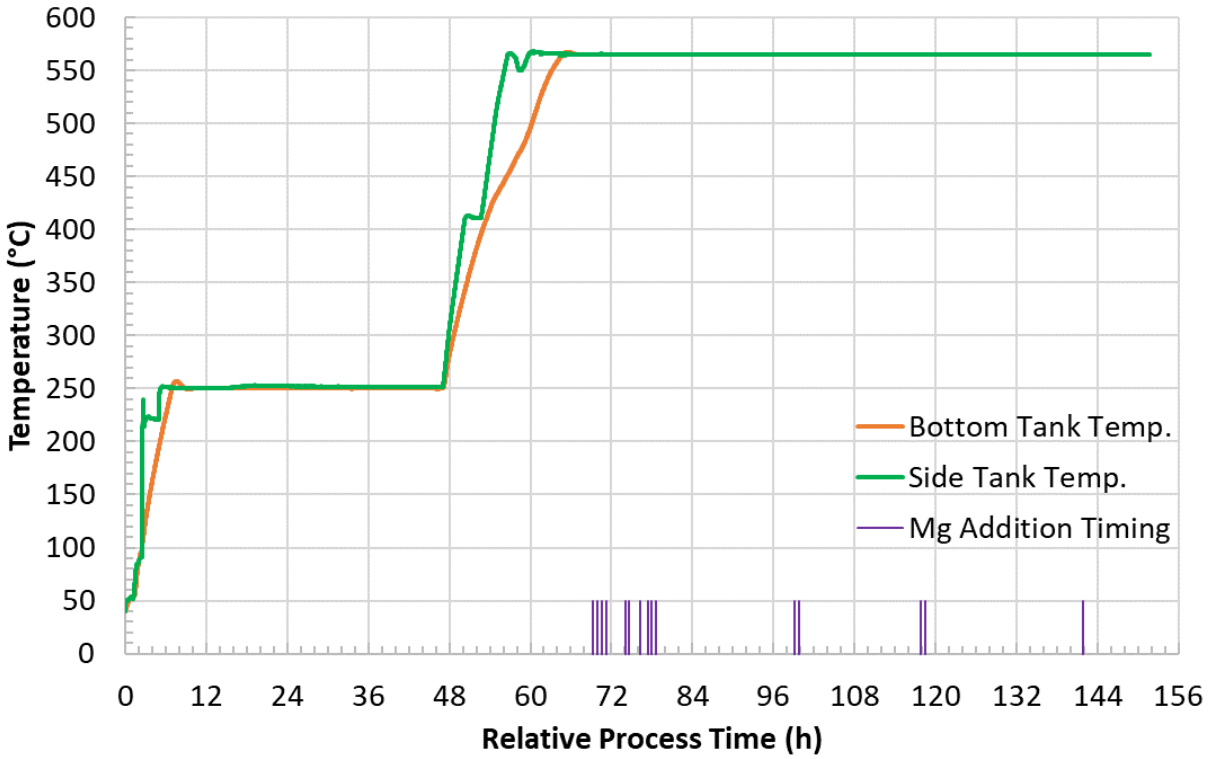

Figure 21. Second purification operation temperature profile and magnesium addition timing.

After the Mg was added, the salt was transferred from the purification vessel to the storage tank. Despite some expected weight loss due to liberation of H_2O and HCl from the loaded salt, the amount of salt transferred (59.6 kg) was greater than the amount loaded (58.9 kg). Approximately 50 mm (2 in.) of salt was left in the purification vessel at the end of the first purification operation. This bottom layer of salt was enriched in MgO and other heavy impurities. Because of the depth of the inserted transfer, some residual salt from the first operation was transferred during the second purification operation.

Little to no debris was found in the three filters after the first batch of salt was transferred. For the transfer of the second batch, only one filter with a nominal 25 µm aperture was included. This reduced the needed driving pressure differential and reduced the risks of leaks and plugging. When the filter was disassembled and inspected after the transfer, only minor signs of debris were found, as shown in Figure 22. The filter was then soaked in a deionized (18 MΩ) water bath for 5.5 h, removed, rinsed with deionized water, and dried. A very fine black particulate was liberated from the filter into the water, and

the filter mass was reduced by 4.7 g during this process. Material samples from the scrubber, filter, and purified salt were taken for future analysis.

Figure 22. Inside of the filter after salt transfer.

3.2 SALT MELTING AND FREEZING

At the end of the initial salt purification, the salt was transferred to the storage tank and frozen. A probe with five thermocouples is located near the center of the vessel; the readings taken by these thermocouples as the salt cooled are shown in Figure 23. At this time, the tank contained 194 kg of salt. The top thermocouple (i.e., thermocouple 5) is suspected to be very near the salt-free surface. Thermocouples 1–4 are connected to the same data acquisition module. At this time, the module was experiencing noise, resulting in approximately 1°C variation in the data before the noise was corrected. Based on the thermocouple responses (i.e., the change in slope and plateauing of the temperature trends) the freezing point is estimated to be 402°C–403°C. Thermocouples 2 and 3 remain hot longer as they're located toward the center of the salt volume.

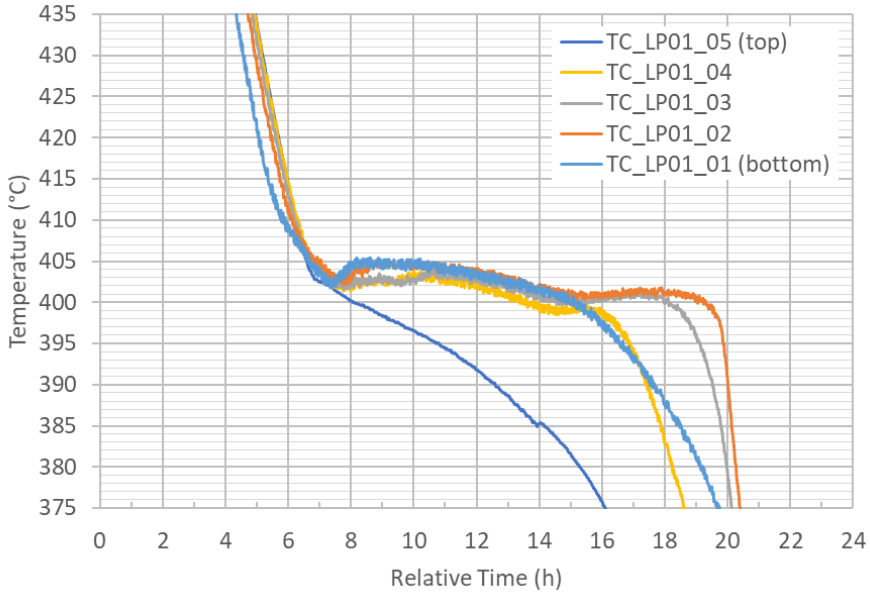

Figure 23. Salt temperatures while freezing in the storage tank after the first purification operation.

In preparation for loop operation, the storage tank was heated to melt the 194 kg of salt. Data for five thermocouples located in the salt are shown in Figure 24. Based on the responses of the top three thermocouples, the melting point is approximately 400°C–402°C. The step-change in temperature for thermocouples 1–4 is indicative of liquid salt movement and contact on the sheath.

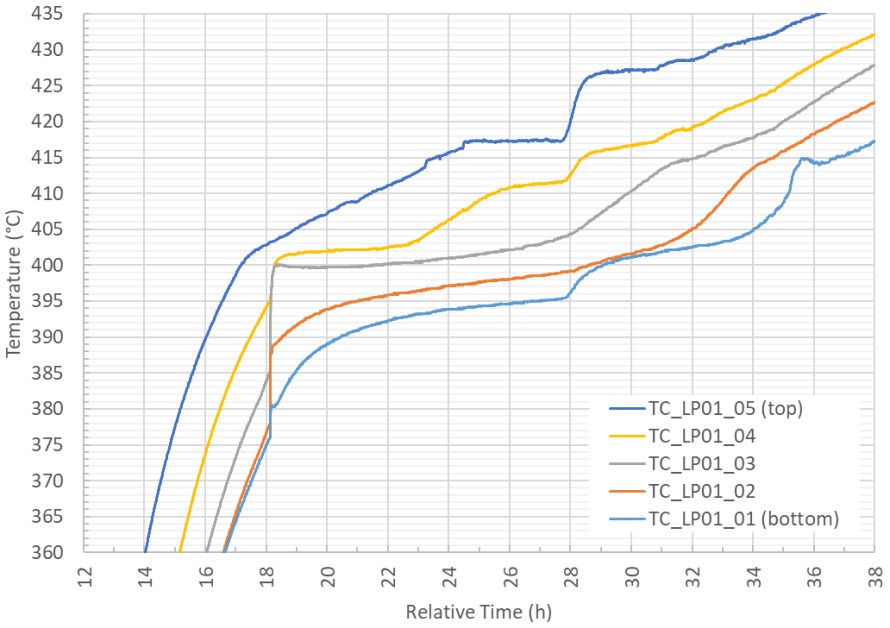

Figure 24. Salt temperatures during melting in storage tank.

At the end of the operation, the salt was transferred to the storage tank and then cooled with a hold point at 434°C. Data for the five thermocouples located in the salt are shown in Figure 25. Based on the cooling rate transition that occurred at approximately 12 h, the salt freezing point is estimated to be approximately 401°C–402°C. These data confirm that the additional salt from the second purification operation did not alter the mixture's melting and/or freezing points.

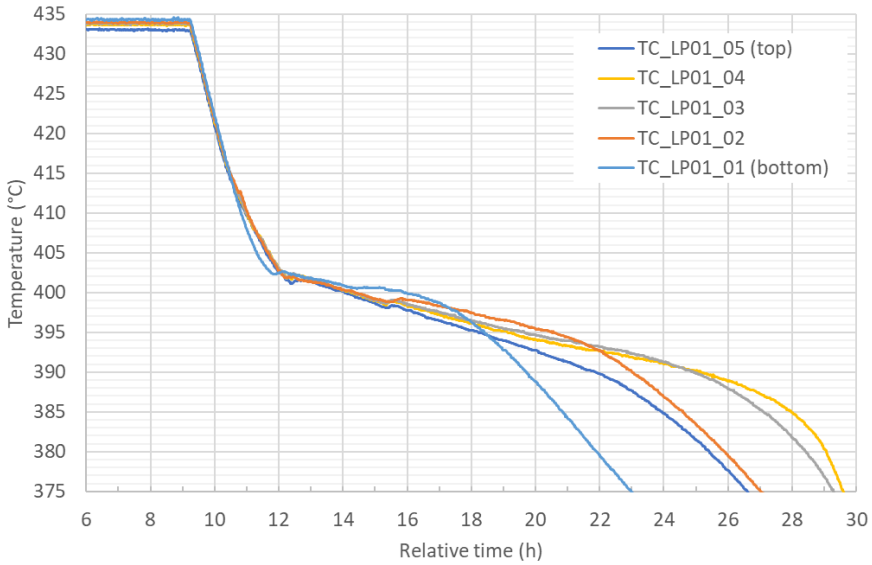

Figure 25. Salt temperatures while freezing in the storage tank.

3.3 LOOP FILLING AND FORMATION OF NATURAL CIRCULATION FLOW

The pump tank is pressurized with Ar to raise the salt into the loop pneumatically. The salt rises simultaneously in both piping legs—the supply side with the main heater and the return side with the heat exchanger—while the displaced gas is vented out of the top port. When the salt reaches the top port, the salt circuit is complete, and the pressures in the pump tank and top port are held constant.

Figure 26 and Figure 27 report the thermocouple responses from the main heater and heat exchanger, respectively, during the filling process. The pressure differentials (converted to units of head) between the pump tank and top port gas spaces are also shown. Due to the large number of thermocouples (i.e., 40) the individual thermocouples are not noted in Figure 26. Thermocouples generally respond by increasing or decreasing in temperature when the salt level approaches their location. The salt's relatively large heat capacity and heat transfer through the structures help to homogenize the system temperatures (see the data in Table 7 of Section 3.4). Based on the thermocouple response, the salt level reached the lowest section of the main heater at approximately 13.87 h and reached the top at approximately 14.01 h. The salt reached the bottom of the heat exchanger tubing at approximately 14.2 h and the top of the tubing at approximately 14.6 h. The main heater temperatures before and after filling are illustrated in Figure 28 and Figure 29, respectively. The illustrations assume front-back and left-right symmetry. The coolest temperatures observed in Figure 26 occur at the bottom and outer edge of the main heater.

Interestingly, both component temperatures were further homogenized during an event starting at 14.8 h. This is the same time that the salt reaches the top port and completes the salt circuit. Comparison of Figure 26 and Figure 27 shows that before the event, the average temperature of the main heater is greater than that of the heat exchanger by approximately 35°C. The salt density difference in these two components, due to the temperature difference, supports formation of natural circulation flow.

The average temperatures of the main heater thermocouples 11 and 32 in the top zone and 13 and 23 in the bottom zone are shown in Figure 30, along with the temperature (i.e., average of six thermocouples) of the inlet supply pipe to the main heater. If an upward flow through the main heater were to occur, one would expect the bottom zone to increase in temperature because the inlet pipe, and salt inside, is at a higher temperature. Also, the top zone would initially cool because of the arrival of the colder salt in the bottom zone and then increase in temperature when the hotter salt from the inlet pipe reaches the zone. Indeed, this response was observed. After 14.8 h, the temperature begins to rise in the bottom zone and then in the top zone 60.0 s later. Based on the distance between the thermocouples and response time, the initial salt velocity is estimated to be 1.58 cm/s in the main heater. Because of the larger flow areas, the velocity is 0.51 cm/s in the piping and 0.12 cm/s in the heat exchanger. These velocities are equivalent to 0.66 L/min of flow through the system. The estimated velocities are reasonable for natural circulation flow.

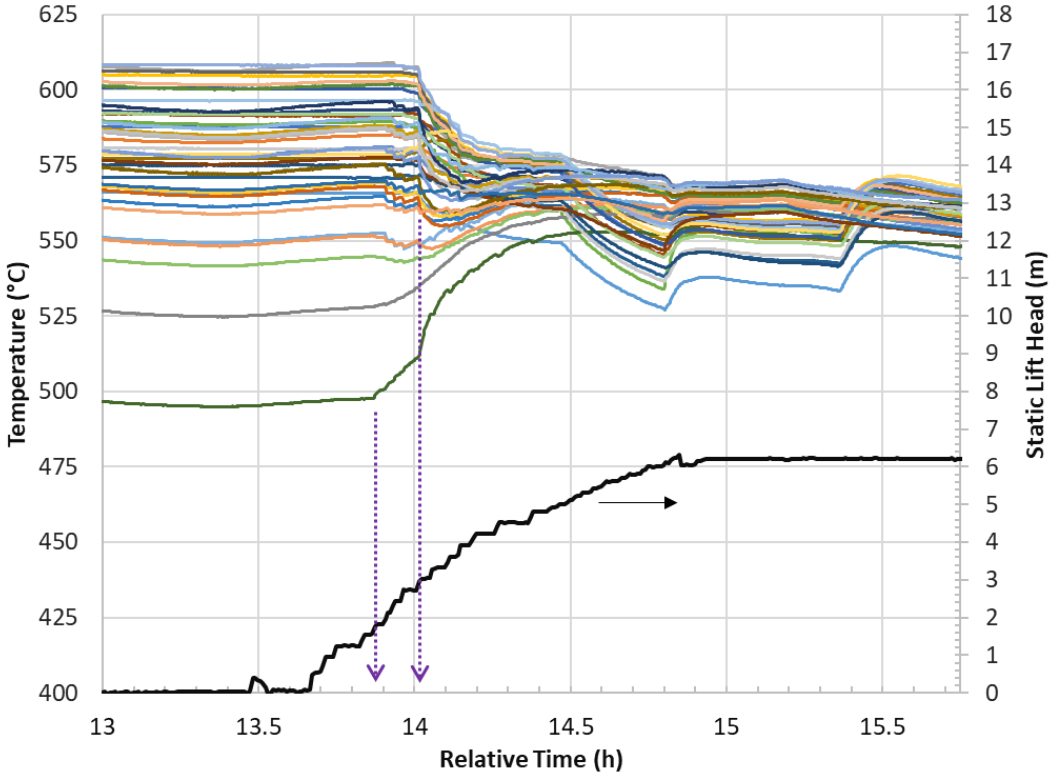

Figure 26. Main heater temperatures, illustrating homogenization, during loop filling.

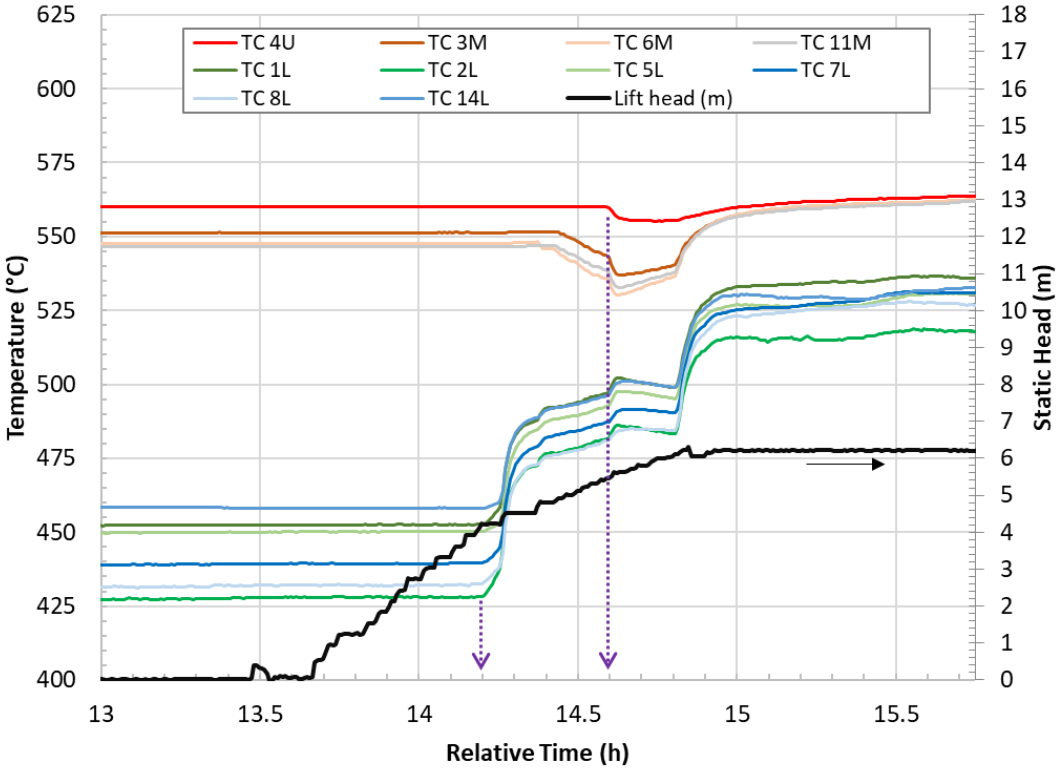

Figure 27. Heat exchanger temperatures during loop filling.

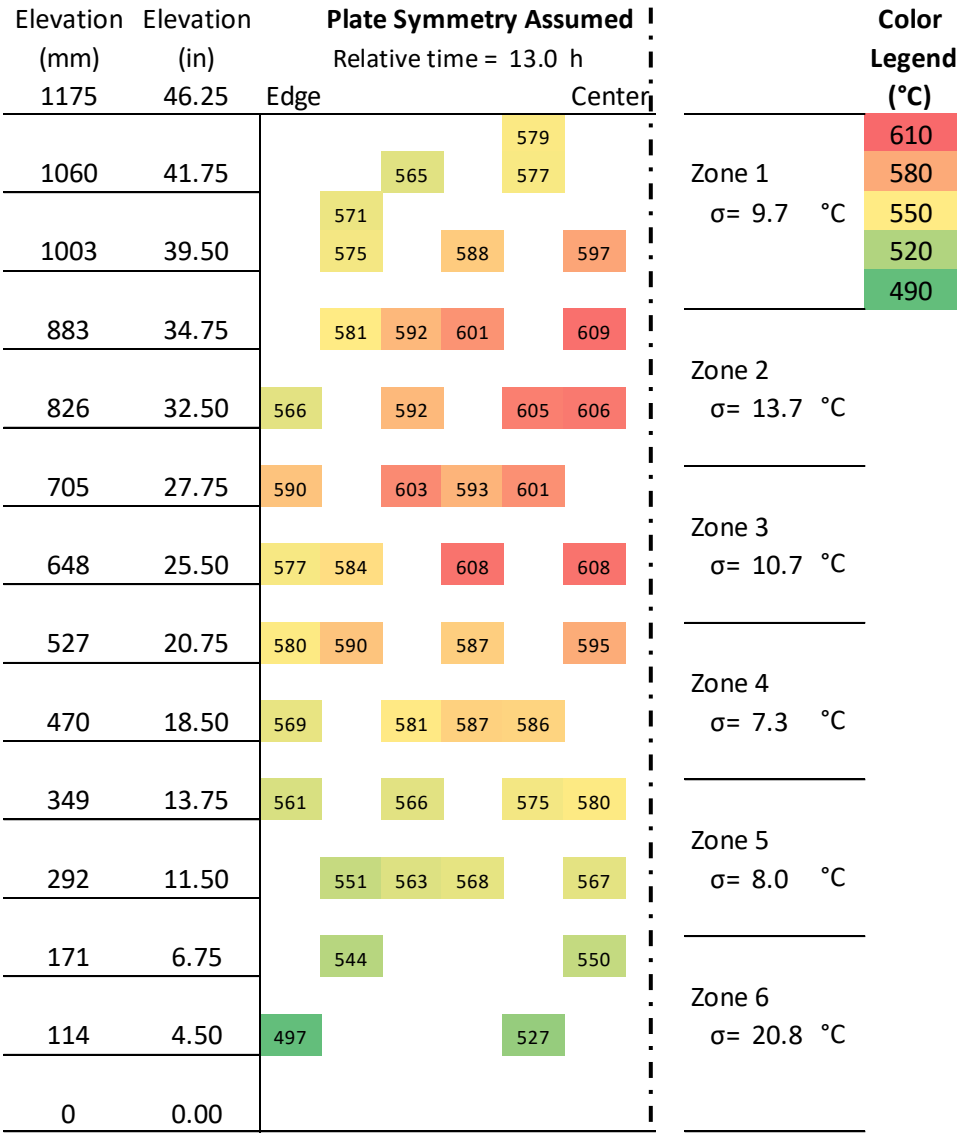

Figure 28. Main heater surface temperatures before salt filling.

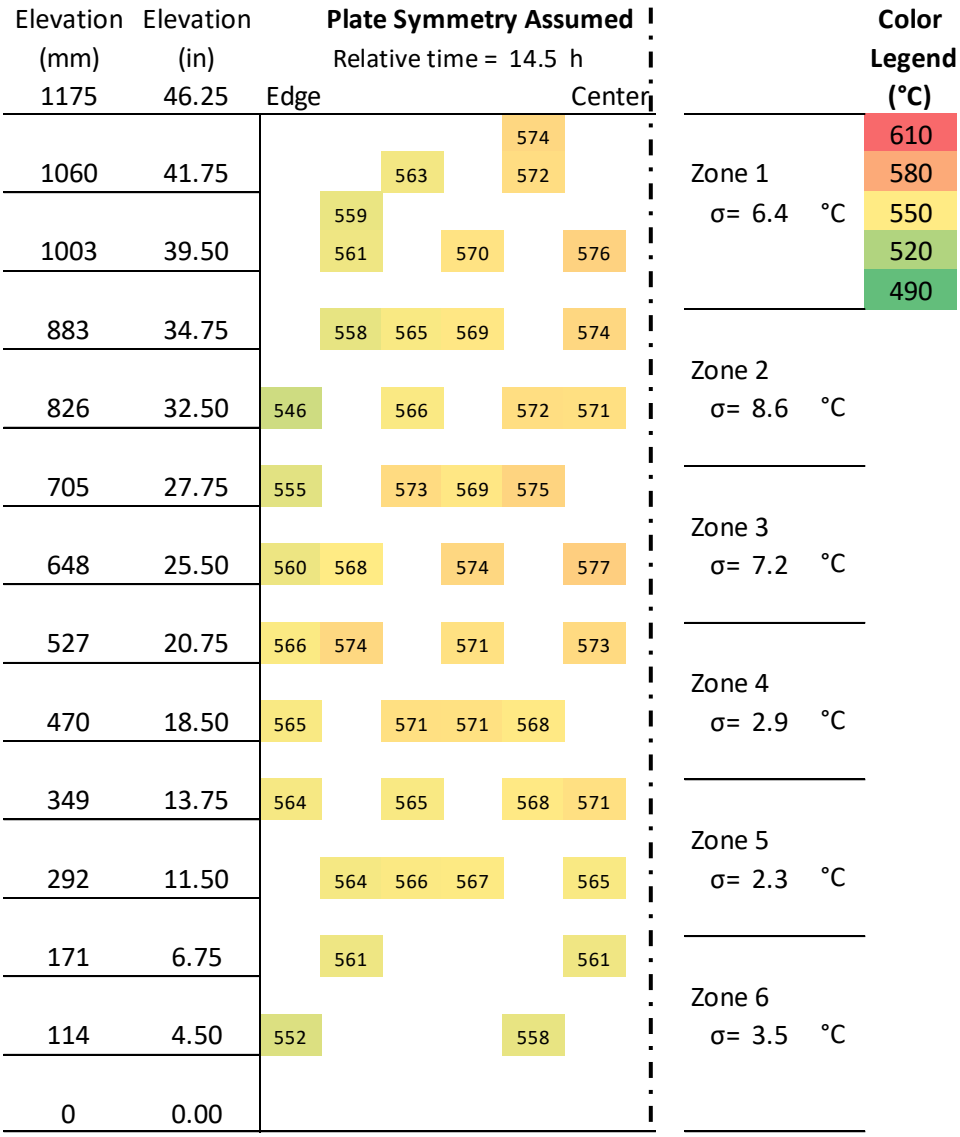

Figure 29. Main heater surface temperatures after salt filling.

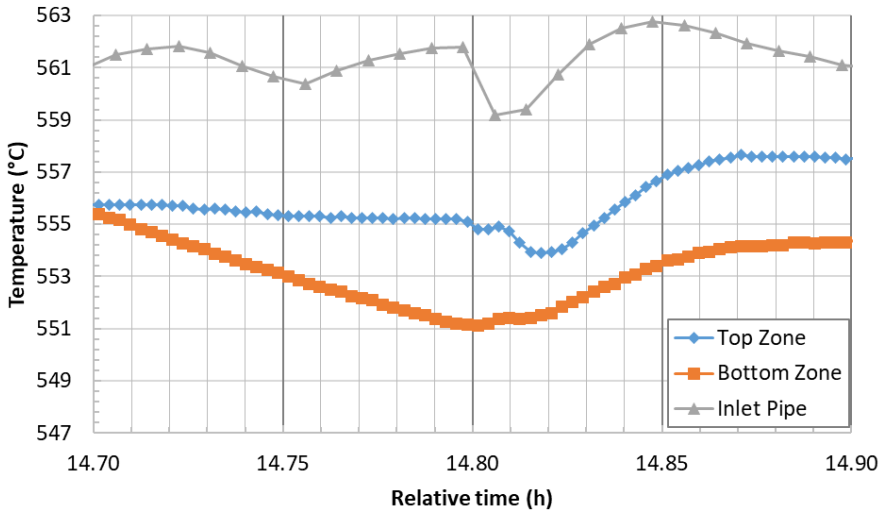

Figure 30. Main heater and inlet pipe temperatures during natural circulation event.

3.4 INITIAL PUMP OPERATION WITH MOLTEN SALT

After the loop was pneumatically filled with salt, the pump was engaged. The pump was operated at four different speeds—34.5%, 39.5%, 45.5%, 49.5%—over the course of 2 h, as shown in Figure 31.

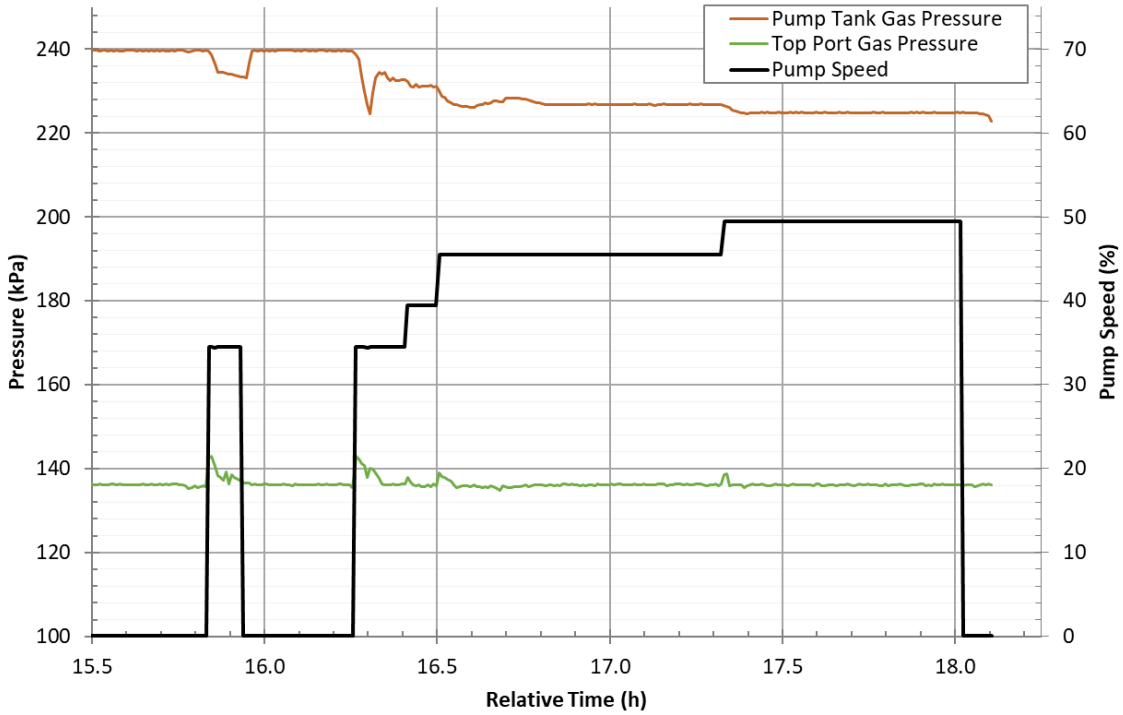

Figure 31. Pump speed and gas space pressures.

After the pump was first turned on at approximately 15.8 h, a pressure response at an electrochemical sensor located in the test port above the main heater prompted the decision to turn it off. No leaks were

found when the flanges and fittings associated with the electrochemical sensor were checked, so the pump was restarted.

Very minor pump vibration was observed during operation. The pump shaft seal gas consumption was within the expected range, and the temperatures monitored below the seal were stable.

As anticipated, the loop temperatures homogenized as the salt was forced through the system, as shown in Figure 32 and Figure 33. Although the trace heating was in operation on the main heater, the temperatures became quite uniform during pump operation, as seen in Figure 34. The temperature variations in the main heater and heat exchanger for various operation states are summarized in Table 7. Despite some uncertainty in the thermal contact of thermocouples on the outer surface of the heat exchanger's finned tubes, the lateral temperature difference toward the bottom of the component homogenized well. Finally, the vertical temperature gradient in the heat exchanger was reduced by half during pump operation. Note that the heat exchanger was enclosed without forced air flow across the component during this operation.

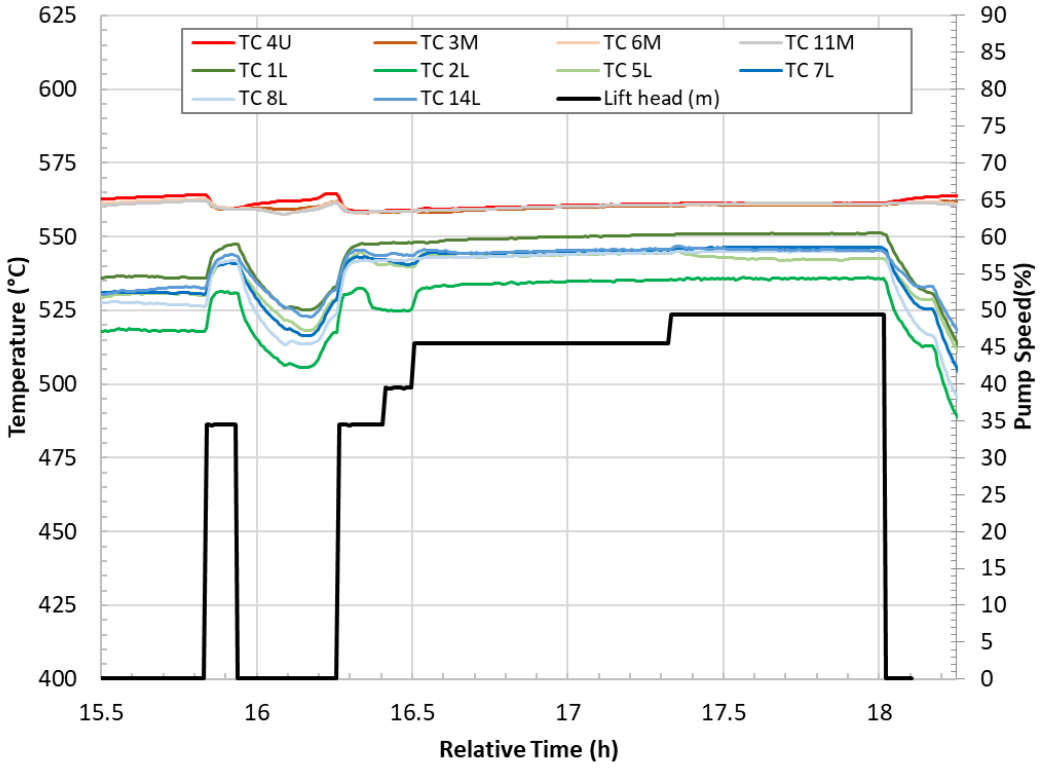

Figure 32. Heat exchanger temperatures during pump operation.

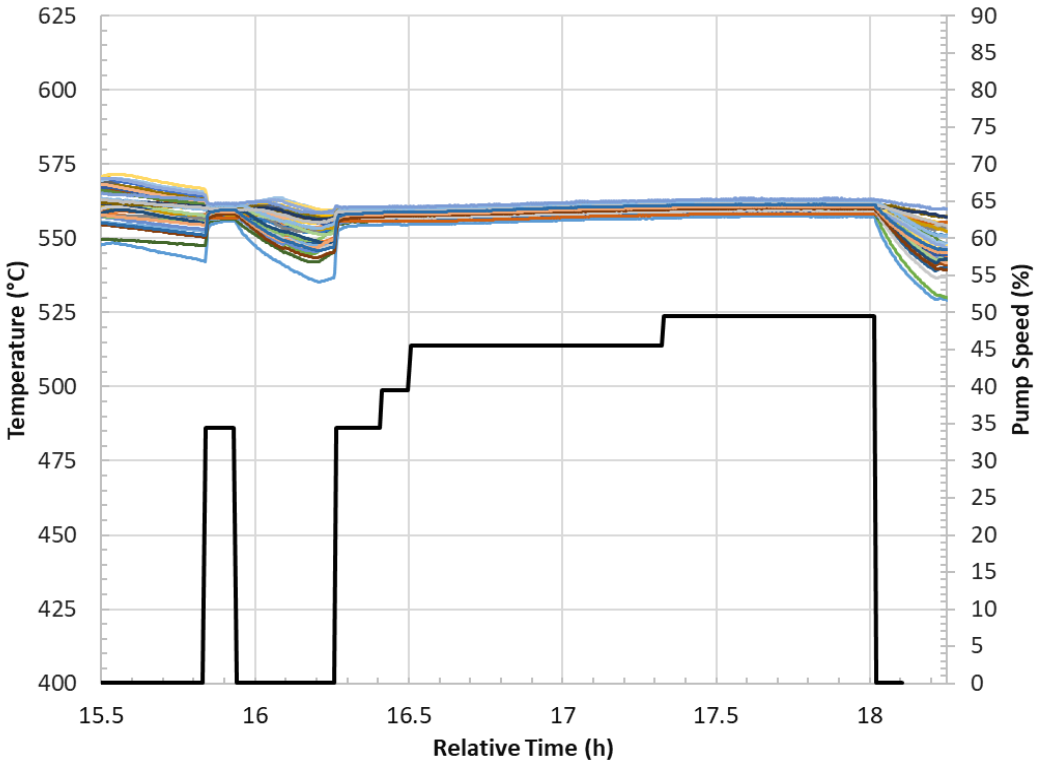

Figure 33. Main heater temperatures during pump operation.

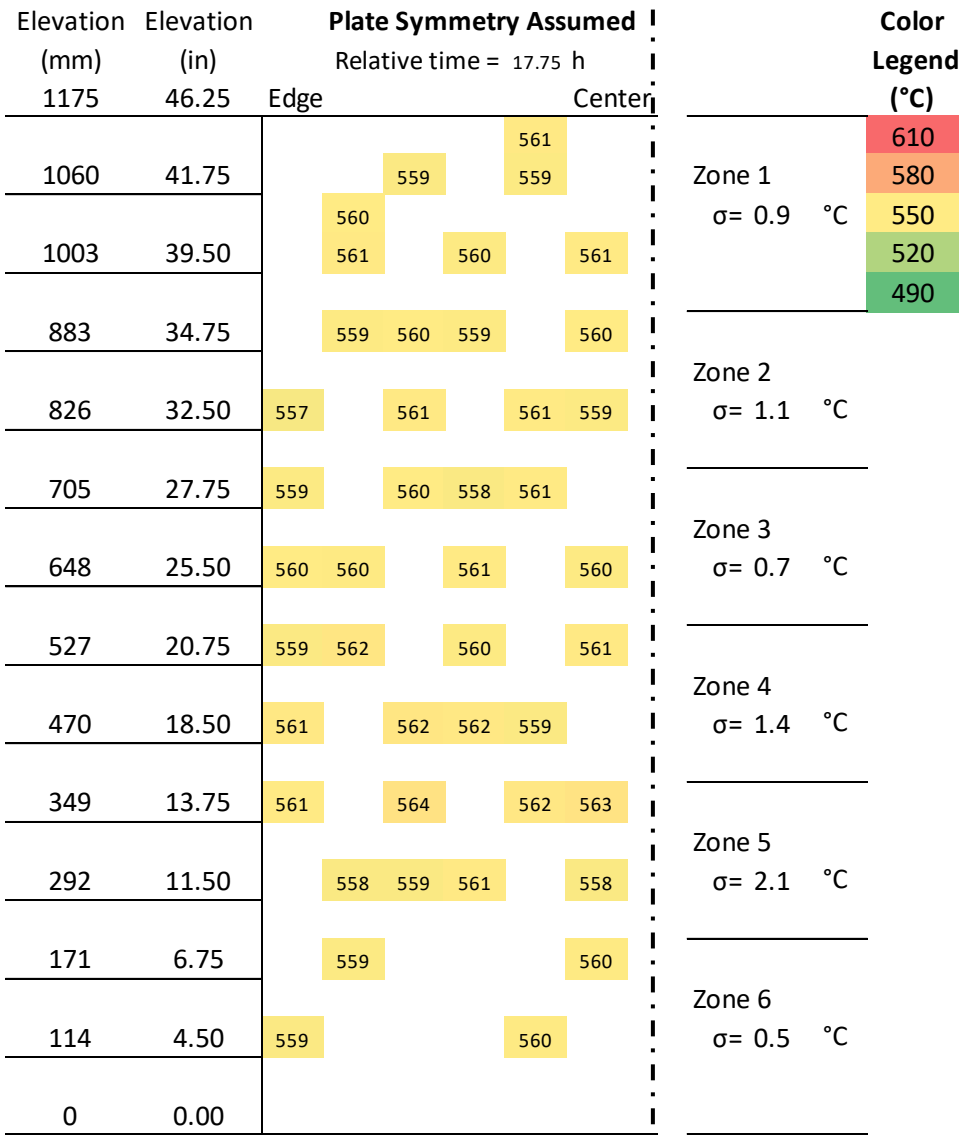

Figure 34. Main heater surface temperatures during pump operation.

Table 7. Component temperature variation during operations

Component	Before filling component at 13 h (°C)	After filling component at 14.5 h (°C)	After filling loop at 15.5 h (°C)	During pump operation at 17.75 h (°C)
Main heater Std. dev. 39 TC	22.5	6.8	5.4	1.2
Heat exchanger Std. dev. lower 6 TC	11.3	6.5	5.5	4.6
Heat exchanger Avg. temp. difference upper-lower TC	117.0	74.0	34.2	17.1

Following the method used to analyze the water test data (see Section 2.1.3), the pressure loss of the flowing salt between the top port and the pump tank (i.e., return side) was evaluated based on the gas pressure data plotted in Figure 35. The average flow losses at the four pump speeds are reported in Table 8. As seen in Figure 35, limited data were taken at pump speeds of 34.5% and 39.5%. The flow losses for these two speeds are based on the average of the last five data points, which span 2 min of operation at their respective speeds. The pump was operated longer at 44.5% and 49.5%, and the flow losses are based on the average of the last 34.5 min of operation at each of these speeds.

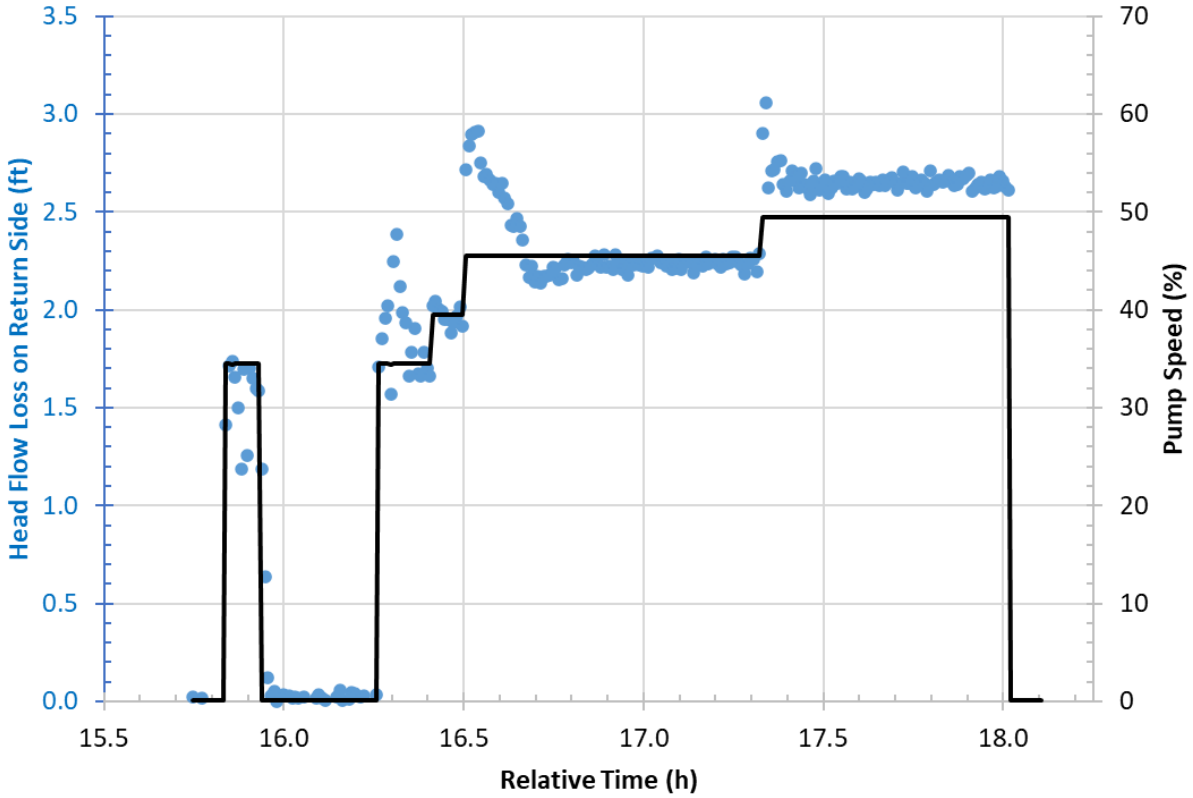

Figure 35. Flow loss data during pump operation.

Table 8. Salt flow loss data and predicted flow rate

Pump speed	**Measured head flow loss on return side**		**Estimated flow rate based on Figure 14**	
%	(ft)	(m)	(GPM)	(l/min)
34.5	1.70	0.517	31.7	120
39.5	1.94	0.592	36.6	139
45.5	2.23	0.681	42.7	162
49.5	2.65	0.807	46.7	177

Figure 36 compares the predicted head flow loss for the return side of the loop with the measured data. As in the water test data comparison, the agreement is better than expected for the salt data given the simple flow loss modeling used for the predictions and thus provides additional confidence and validation of the predicted system characteristics. Based on the confidence in the system characteristics presented in Figure 14, the predicted system flow rates at the four pump speeds are presented in Table 8. These predicted flow rates can be compared with future flow meter readings.

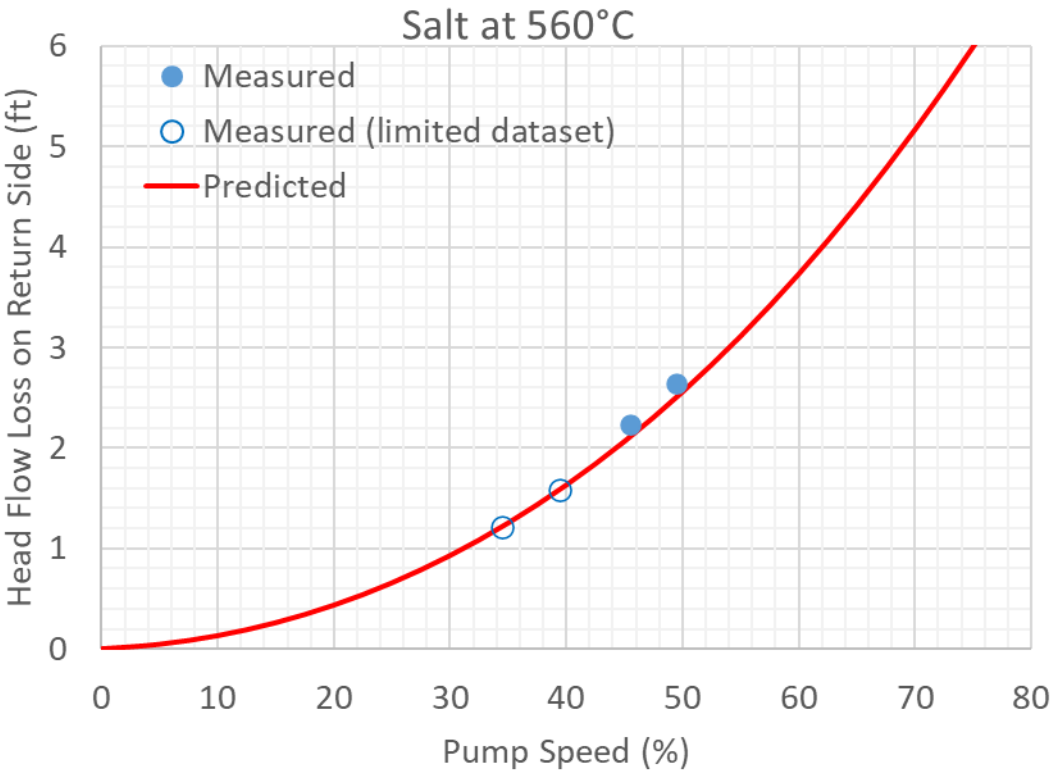

Figure 36. Comparison of the predicted and measured head flow loss in the return side of the loop for the salt test data.

4. FUTURE LOOP OPERATION

The initial test plan [4], is summarized in Table 9. The testing described in Section 2 marks the completion of shakedown testing of the installed system.

Loop operation has progressed to the startup phase. Isothermal losses have been estimated (Section 2.2). The salt composition was measured after the initial purification process [3], and future salt sampling is planned to track and verify the composition over time. Pressure and temperature readings were checked, and initial electrochemical measurements were taken. However, the salt flow rate remains to be verified to enable quantified heat transfer testing and verification of the molten salt pump curve. The ability of the system to maintain steady level and thermal conditions was verified during the initial flowing operation. This testing also yielded valuable operations experience and useful insight into the system characteristics. The startup-phase testing also supports the planned test campaigns, providing run time and exposure of corrosion coupons in the loop. Future operations will progressively advance to higher system temperatures.

Near-term plans are to collaborate with industry partners to test salt sensors in the loop. A new test campaign to investigate natural circulation flows was added in response to the startup testing. In addition to the test campaigns listed in Table 9, the design report notes several more potential areas of investigation: testing components such as salt-to-sCO_2 heat exchangers, salt valves, and instrumentation; investigating off-gas and vapor pressure effects; refining the purification processes and online REDOX control; validating digital models; and gaining experience with high-temperature salt system handling, operation, and maintenance. In the near term, the anticipated focus will be:

- Gaining system operation experience
- Characterizing the system operation envelope
- Exposing corrosion coupons
- Exercising the system's electrochemical and other sensors
- Testing novel instrumentation provided by a commercial partner

Table 9. Initial test plan

Phase: Shakedown **Purpose: ensure subcomponents meet performance expectations before salt introduction**	
I&C verification	Verify temperature, gas pressure, gas flow rate sensor readings
Heater operation	Verify individual heater integrity
Pump operation dry	Run dry, take up to speed, and balance as needed
Heat exchanger operation	Verify fan operation
System leak check (gas, room temperature)	Leak check fittings, flanges, etc., at low temperatures
Heat system: isothermal	Ensure the ability to maintain system temperatures; estimate heat losses
System leak check (gas, high temperature)	Leak check fittings, flanges, etc., at high temperatures
System trips	Verify preset system trips to the extent possible
Pump operation wet	Run system with water and verify pump operation and system controls
Phase: Startup **Purpose: characterize integral system behavior and determine the system operational envelope**	
Salt characterization	Perform baseline measurements of salt composition, impurities, electrochemical potential
I&C verification	Verify flow rate, pressure, level sensor, and electrochemical sensor readings
Isothermal operation	Ensure the ability to maintain system temperatures while salt is flowing; estimate zone heat losses
Heater performance	Verify heat transfer vs. input power for salt flow rate (3–6 kg/s) and inlet temperature (500°C–700°C)
Pump performance	Verify pump curve to system capabilities (3–6 kg/s)
Heat exchanger performance	Verify heat transfer vs. fan speed and door location for salt flow rate (3–6 kg/s), inlet temp. (525°C–725°C)
System trips	Revise preset system trips based on the operational envelope
Phase: Test Campaigns **Purpose: obtain quality scientific data**	
Corrosion control demonstration	Conduct coupon tests: 2 × lines (1 × hot leg, 1 × cold leg) of 12 samples (6 × C-276, 6 × Inconel 600); conducted over 100 and 200 h In-situ corrosion measurement (as applicable)
Natural circulation flow	Investigate the formation and flow rate of natural circulation under a variety of temperature differentials
Heat transfer in main heater and heat exchanger	Test heat transfer vs. fan speed, salt flow rate (3–6 kg/s) Reynolds number (15,000–50,000), salt inlet temp. (500°C–700°C)
REDOX control system and oxygen/impurity sensors demonstration	Demonstrate reduction and control of oxygen/impurities using the REDOX control system as applicable (e.g., getter can, electrochemical oxygen removal). This testing will occur over the course of other planned tests and could include intentional introduction of impurities.
Extended operation demonstration	Demonstrate system robustness through extended runs with salt circulating in the system >500°C and a >25°C temperature gradient.

5. COMPARISON OF FASTR TO OTHER CHLORIDE SALT FACILITIES

In contrast to facilities using fluoride salts, very few forced-circulation molten chloride salt loops have operated. Four facilities other than FASTR were identified in the open literature. Brookhaven National Laboratory (BNL) operated a loop (Loop M) for a ternary mixture of $MgCl_2$-KCl-NaCl in 1957 [7, 8, 9], when BNL was developing technology to support nuclear reactor fuel processing as part of the Liquid Metal Fuel Reactor program. Unfortunately, limited data are available on the completed loop design and testing. However, insights from the development and testing of components are discussed in Raseman et al. [7], and results of the corrosion study with the loop are discussed in Susskind et al. [8]. Another chloride salt forced-circulation loop was operated at the University of Wisconsin (UW). J. Ambrosek developed the loop as part of his dissertation to measure heat transfer in binary KCl-$MgCl_2$ salt [10]. Another loop, the molten salt dynamics rig (MSDR), was developed by UK National Nuclear Laboratory to investigate pumping technologies for LiCl-KCl [11]. Finally, a forced-circulation loop was recently constructed and operated at the University of Arizona (UA) to measure the heat transfer characteristics of a ternary blend of NaCl-KCl-$ZnCl_2$ [12, 13] with a low melting point. Other molten chloride salt forced-circulation facilities may have operated, but their designs and operations could not be found in the open literature.

High-level design details and operation histories of the four facilities are compared in Table 10. Details from the first operation and the facility design for FASTR are also noted in the table. It should be stressed that there is limited information available on the other facility designs and their operation histories.

In all four of the other facilities, stainless steel was used as a primary construction alloy. In addition to stainless steel, UA used alloy C-276 for the main flow tubing. FASTR was constructed primarily of alloy C-276 except for the main heater, which was constructed of alloy 600, as were the thermocouple array sheaths in contact with the salt. Literature demonstrates that alloy C-276 is a salt-compatible and high-strength material [4]. Ongoing research in chemistry control and corrosion testing are investigating the feasibility of stainless steel for high-temperature chloride salt systems [14].

The four facilities have flow rates ≤15.9 GPM and are notably smaller than FASTR. With the lower flow rates, the inner diameters of the main piping and tubing are 0.62–1.05 in. (15.7–26.7 mm), whereas FASTR uses piping with a 2.07 in. (52.5 mm) inner diameter. The lower flow rates facilitate using less salt volume. The other facilities contained approximately 2.2–7× less salt.

The UK NNL loop and BNL loop was operated at relatively low temperatures, 400°C–500°C and 515°C–520°C, respectively. The UW loop heat transfer tests covered a broad range of temperatures up to 775°C. Finally, the UA heat transfer tests covered 400°C–600°C. Although the design point for the hot side of FASTR is 725°C, the first operation was implemented at 560°C. This temperature is higher than that used for the Loop M and MSDR operation but lower than the peak temperatures achieved for the UA and UW heat transfer tests.

The four loops operated under relatively low power. The power of the UK NNL loop and BNL loop were not reported, but they were operated near isothermal conditions, thus eliminating the need for a high-power test section. Although the UW and UA loops used heated test sections for their heat transfer measurements, their single-tube geometry and test conditions required less than a couple of kilowatts of power. The first operation of FASTR was under isothermal conditions; however, the loop was specifically designed with a high-power (i.e., >300 kW) heated section to facilitate heat transfer studies and to generate a temperature gradient across the system for use in corrosion studies.

The other facilities accrued 2.75–70 days of operation time. Although these operation times are lauded, pumps for fluoride salt applications historically accrued 96 years of operation time [15], and existing

loops are continually adding to the knowledge base. With future operations planned, FASTR will continue to expand the operation knowledge base for forced-circulation molten chloride salt systems.

Table 10. Comparison of FASTR with other forced circulation chloride salt loops

Organization	BNL (Loop M) [7, 8, 9]	Univ. of Wisconsin [10]	UK NNL (MSDR) [11]	Univ. of Arizona [12, 13]	ORNL (FASTR)
Year	1957	2011	2004-2006 2013-2015	2022	2022
Salt	$MgCl_2$-KCl-NaCl	KCl-MgCl2	LiCl-KCl	NaCl-KCl-ZnCl2	$MgCl_2$-KCl-NaCl
Primary alloy of construction	347 SS	316 SS	316 SS	C-276 piping SS components	C-276, 600
Primary studies	Components, corrosion	Heat transfer	Pumping methods	Heat transfer	Components, corrosion, heat transfer
Salt volume	NA (≤42 L[a])	NA (≤22 L[b])	71.4 L[e]	22 L	154 L
Primary loop diameter	1/2” sch 40 pipe	1” tube	1” pipe	1” tube, 0.065” wall	2” sch 40 pipe
Operation temperature	515°C–520°C	475°C–775°C	400°C–500°C	400°C–600°C	560°C (1st operation) 450°C–725°C (design)
Operation time	1690 h	>500 h	66 h[e]	~264 h (11 days)	~2 h (1st operation) ~2 years (design)
Flow rate	11 GPM at 44.5 ft head 1.5–7 GPM, ≤17 ft head	<1 GPM[c]	4.8 GPM at 1.7 ft head to 15.9 GPM at 21.7 ft head	≤10 GPM	32 GPM at 11 ft head to 47 GPM at 23 ft head (1st operation[d]) 30–70 GPM (design)
Thermal Power	NA (isothermal)	≤4 kW	NA (isothermal)	~1.5 kW to test section	Isothermal (1st operation) 400 kW (design)

NA: Not available

[a] A quarterly report notes a 150 lb batch (approximately 42 L) of salt was being prepared for Loop M and other studies [9]. The estimated size of the dump tank based on the image in Susskind et al. is consistent with this volume of salt [8].

[b] This volume is an estimate based on the reported 12” pipe used for the pump sump tank and a height estimated from the salt loop image in Ambrosek [10].

[c] Based on the Reynolds numbers tested, the flow through the test sections was 0.20–0.02 GPM; however, the reported pump testing shows the pump was capable of flow rates greater than 5 GPM [10].

[d] Based on Figure 14 for the operated pump speeds.

[e] Based on 500°C. Only 66 h of operation is noted, with 2 h of centrifugal pump operation time [11].

6. CONCLUDING REMARKS

FASTR is a state-of-the-art molten chloride salt facility with appreciable pumping capacity, thermal power, and temperature capabilities. A range of testing was completed to support the commissioning of the system. With the successful start of forced-circulation salt operations, the facility has transitioned into the startup phase. To date, several activities that were predefined for the startup phase have been completed. Highlights of the reported progress include the following:

- The forced-flow loop was successfully operated with molten chloride salt for the first time.
- An additional 58 kg of salt was purified and added to the loop, bringing the total loop salt volume to 154 L. The purification process was accelerated over that of the previous operation and progressed without disruption.
- Melting and freezing of the ternary salt were observed at 400°C–402°C.
- Isothermal heat loss as a function of temperature was measured for 49 heater zones. Heat loss data at the component level were also obtained. Heat losses from the heat exchanger enclosure were higher than anticipated during the design phase.
- The system maintained temperatures sufficiently above the melting point to prevent salt freezing.
- The system maintained stable gas pressures and liquid levels during water and salt testing.
- The pump curves (i.e., flow rate vs. head at various speeds) were validated through water testing by the pump manufacturer and through independent tests performed by ORNL.
- The pump operated with little to no vibration during water testing and molten salt operation.
- During salt operations, the pump was exercised at four speeds (34.5%–49.5%), producing estimated flow rates of 120–177 L/min (32–47 GPM) and 3.4–7.0 m (11–23 ft) of head.
- Pressure drop measurements for the return side of the loop agreed well with predictions for water and molten salt operation. This agreement provides confidence in the prediction methodology. This methodology was also used to predict the total system pressure drop and system flow rate as functions of pump speed.
- As expected, variations in loop temperatures decreased after filling the loop with salt and further decreased upon initiation of pumped flow. During pump operation, the standard deviation in temperature was 1.2°C throughout the main heater and 4.6°C laterally across the bottom of the heat exchanger.
- During salt operations, a natural convective flow in the loop is suspected to have occurred upon complete filling of the flow circuit. This slow flow homogenized the system temperatures before pump operation.
- Leak checking prior to operation identified some leak points, which were addressed. No gas or salt leakage was identified during salt operation.

Very limited forced-circulation testing of molten chloride salts is documented in the literature (see Section 5). The startup of FASTR has added to this experience base. New findings from future loop operations are anticipated; nevertheless, the facility at its current stage is a significant step in the advancement and de-risking of high-temperature chloride salt technology.

7. REFERENCES

1. Mehos, M. et al. 2017. *Concentrating Solar Power Gen3 Demonstration Roadmap*. National Renewable Energy Laboratory, Golden, Colorado.
2. Robb, K. R., P. Mulligan, G. Yoder, Jr., K. Smith, and J. Massengale. 2019. *Facility to Alleviate Salt Technology Risks (FASTR): Preliminary Design Report with Failure Modes and Effects Analysis*. ORNL/TM-2019/1370, Oak Ridge National Laboratory.
3. Robb K. R., S. Baird, J. Massengale, N. Hoyt, J. Guo, and C. Moore. 2022. *Engineering-Scale Batch Purification of Ternary $MgCl_2$-KCl-NaCl Salt Using Thermal and Magnesium Contact Treatment*. ORNL/TM-2022/2554, Oak Ridge National Laboratory.
4. Robb, K., S. Baird, J. Massengale, E. Kappes, and P. Mulligan. 2022. *Facility to Alleviate Salt Technology Risks (FASTR): Design Report*. ORNL/TM-2022/2803, Oak Ridge National Laboratory.
5. White, F. M. *Fluid Mechanics*. 5th ed. Boston Mass: WCB/McGraw-Hill; 2003.
6. Zhao, Y. 2020. *Molten Chloride Thermophysical Properties, Chemical Optimization, and Purification*. NREL/TP-5500-78047, National Renewable Energy Laboratory, Golden, Colorado.
7. Raseman, C.J., H. Susskind, G. Farber, W.E. McNulty, and F.J. Salzano. 1960. *Engineering Experience at Brookhaven National Laboratory in Handling Fuse Chloride Salts*. BNL 627 (T-192), Brookhaven National Laboratory.
8. Susskind, H. et al. 1960. *Corrosion Studies for a Fused Salt-Liquid Metal Extraction Process for the Liquid Metal Fuel Reactor*. BNL-585, Brookhaven National Laboratory, Upton, New York.
9. Maslan, F. 1958. *Nuclear Engineering Department Progress Report for May 1–September 30, 1957*. BNL-477, Brookhaven National Laboratory, Upton, New York.
10. Ambrosek, J. W. 2011. "Molten Chloride Salts for Heat Transfer in Nuclear Systems." PhD diss., University of Wisconsin, Madison.
11. Mullen, Eve, et al. "Transfer characteristics of a lithium chloride–potassium chloride molten salt." *Nuclear Engineering and Technology* 49.8 (2017): 1727-1732.
12. Zhang, Y. 2022. "Investigations of Heat Transfer and Entropy Production of High Temperature Molten Chloride Salts Circulation in Concentrating Solar Power Systems." PhD diss., University of Arizona.
13. Zhang, Y. et al. 2022. "Experimental Study of Eutectic Molten Salts NaCl/KCl/ZnCl2 Heat Transfer Inside a Smooth Tube for High-Temperature Application." *Journal of Solar Energy Engineering* 144(4): 044501.
14. Gong, Q. et al. 2022. "Molten Chloride Salt Technology for Next-Generation CSP Plants: Compatibility of Fe-Based Alloys with Purified Molten MgCl2-KCl-NaCl Salt at 700°C." *Applied Energy* 324: 119708.
15. Robb, K., P. Jain, and T. J. Hazelwood. 2016. *High-Temperature Salt Pump Review and Guidelines – Phase I Report*. ORNL/TM-2016/199, Oak Ridge National Laboratory.